Ph.D. Dissertation of Christine Haewon Park

# Roles of inner wall residues of pore domain in the voltage-dependence and $Ca^{2+}$ permeability of TRPC1/4 heteromeric channel

## TRPC1/4 이형복합체의 전압의존성과 칼슘투과도에 대한 이온통과부위 내측벽 아미노산 잔기의 역할

August 2023

Graduate School of Medicine
Seoul National University
Biomedical Sciences Major

Christine Haewon Park

# Roles of inner wall residues of pore domain in the voltage-dependence and $Ca^{2+}$ permeability of TRPC1/4 heteromeric channel

Insuk So

Submitting a Ph.D. Dissertation of
Biomedical Sciences

April 2023

Graduate School of Medicine
Seoul National University
Biomedical Sciences Major

Christine Haewon Park

Confirming the Ph.D. Dissertation written by
Christine Haewon Park
July 2023

Chair _____(Seal)
Vice Chair _____(Seal)
Examiner _____(Seal)
Examiner _____(Seal)
Examiner _____(Seal)

# Abstract

The family of transient receptor potential (TRP) channels is involved in diverse biological processes, and their significance in physiological context has spiked research in the field in the last two decades. The TRPC subfamily of transient receptor potential channels consist of 7 subtypes, where TRPC1, 4, 5 and TRPC 3, 6, 7 are grouped according to sequence homology.

TRPC1 and TRPC4 are proteins belonging in the same group under TRPC channel family and the two are known to form a heterotetrameric channel. TRPC4 can form a homotetrameric, non-selective cation channel by itself, and is expressed in many cells and tissues including neurons, smooth muscles, cardiac cells, skeletal muscle cells, kidney and immune cells. TRPC1 on the other hand is expressed almost ubiquitously in all tissues. Unlike the TRPC4 homomer, the involvement of TRPC1 subunit in the heteromer changes several major characteristics of the channel. In this study, I focused on the pore region (selectivity filter, pore helix, and S6 helix) of TRPC1 and TRPC4 as a determinant of the identity and major characteristics of a heteromeric TRPC1/4 channel: decreased calcium permeability of the channel and outward-rectifying I-V curve.

Mutants and chimeras of the pore residues were

created and their currents were recorded using whole-cell patch clamp under a potent TRPC4 agonist Englerin A stimulation. The lower gate mutants of TRPC4 (I617V, N621H and IN→VH) exhibited diminished calcium permeability as measured by GCaMP6s fluorescence. TRPC4 single mutants (G577S and N580H) and the double mutant (GN→SH) of the selectivity filter maintain a double rectifying I-V shape, but the magnesium block induced plateau is shifted upwards. Single mutations (I617V and N621H) and double mutations (IN→VH) of the TRPC4 lower gate residues have no effect on the I-V curve shape of the channel. When all of the selectivity filter and lower gate residues are mutated (GNIN→SHVH), Englerin-A induced current is greatly diminished.

TRPC1 mutants were made vice versa to analyze the roles of TRPC1 pore residues on the heteromer's characteristics. Single mutations of the TRPC1 pore region (S600G, H603N, V642I and H646N) are insufficient to change the I-V curve shape of the heteromeric channel. However, chimeric channels substituting the pore region of TRPC1 to TRPC4 produced a double rectifying I-V curve shape characteristic to that of a TRPC4 homomeric channel.

The change in calcium permeability and rectification of the channel is controlled by the pore residues of the TRPC1/4 heteromer, and these results

suggest TRPC1/4 heteromers are able to fine-tune the excitability of the cell in a physiological context depending on its expression. Continued research on heteromers will broaden the scope of means of channel modulation and provide new insight into drugs and therapeutics research.

**Keyword :** TRPC4, TRPC1, heteromeric TRP channels
**Student Number :** 2020-36583

Published in *American Journal of Physiology-Cell Physiology*

**Park CH, Kim J, Lee JE, Kwak M, and So I.** Pore residues of transient receptor potential channels canonical 1 and 4 heteromer determine channel properties. *Am J Physiol Cell Physiol* 325: C42-C51, 2023.

# Table of Contents

# List of Figures

# 1. Introduction

The molecular structure, biological function, physiological significance, and its role in pathology has become an increasing area of research in transient receptor potential (TRP) channels in the last two decades. TRP channels are involved in and are essential in numerous cell functions, and its role under different biological context is only beginning to become demystified, owing to the development of new experimental tools.

## TRPC4 channel and its expression

Under the TRPC channel subfamily, there are 7 subtypes of TRPC channels. Based on sequence similarity, TRPC3, 6 and 7 are grouped together whereas TRPC1, 4 and 5 are grouped together as another subgroup (1). TRPC1 is known to be almost ubiquitously expressed in mammalian tissues, whereas TRPC4 and TRPC5 have a limited expression pattern. TRPC4 is expressed in various organs and cell types, including brain (2, 3), gastrointestinal tract (4, 5), heart (6, 7), lungs (5, 6) and kidney(8, 9) (Figure 1). Recently, Kollewe et al. (2023) showed that TRPC4 and TRPC5 homotetramer existed as minor, but more heterotetramers existed in the brain with multi-epitope affinity-purification and nano-LC-MS/MS (10). Even among the heterotetramers, TRPC1/4, TRPC1/5 and TRPC1/4/5 heterotetramers were found in the brain but not TRPC4/5 heterotetramers.

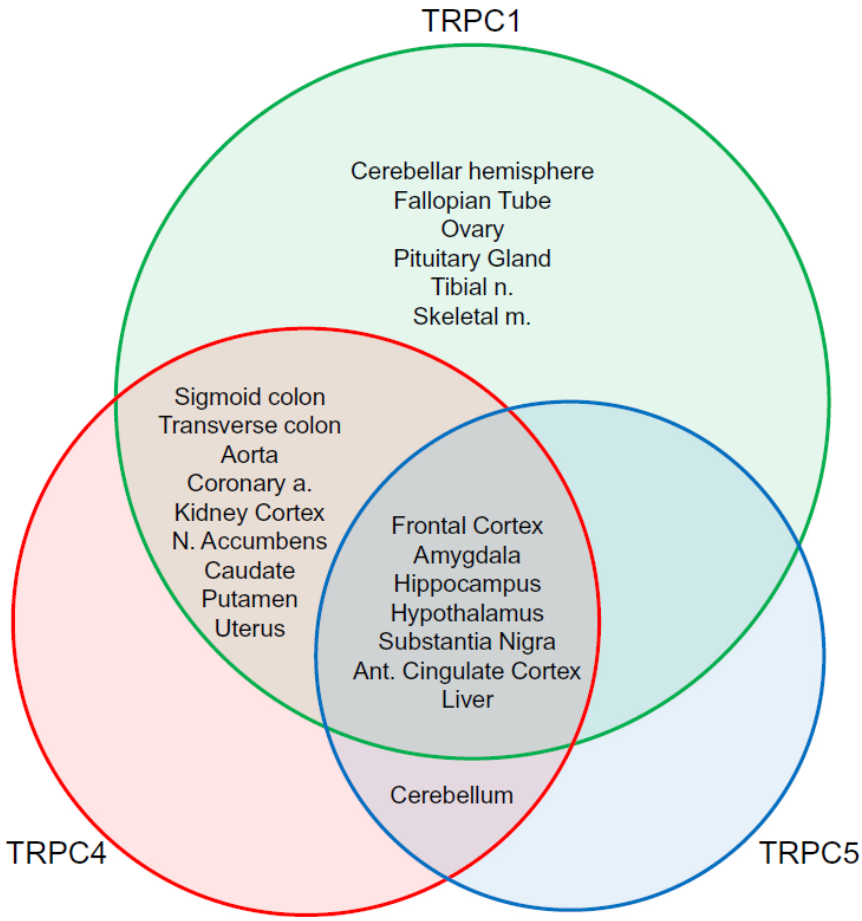


**Figure 1.** Tissue distribution of TRPC1, 4 and 5 channels and the overlapping expression patterns are shown (11).

## Structure of the TRPC4 channel

TRPC4 shares the core structural characteristics of the TRP channels comprising of 6 transmembrane domains, a putative pore forming domain between transmembrane domain 5 and 6, and C-terminus and N-terminus located in the cytosolic region (1). From the N-terminus, there are four ankyrin repeat domains (ARD) which are important in multimerization, membrane trafficking and protein folding, which is then followed by the helix-loop-helix (HLH) domain consisting of seven alpha helices (Figure 2). The HLH domain is then connected to the voltage sensor like transmembrane domain via pre-S1 helix, followed by the last two transmembrane helices containing the pore helix (12). TRPC5 channel has the similar structure to TRPC4. The C terminal region and the pore domain of TRPC5 were quite different from that of TRPC4. The pore domain of TRPC5 has additional amino acids between S5 and S6 and plays important roles of the activation and inactivation time course by TRPC4/5 activator Englerin A. TRPC1 structure was not revealed but the homology between TRPC1 and TRPC4 is high when the amino acids from ARD to coiled-coil domain (CCD) are compared. The homology model of TRPC1 from TRPC4/5 structure was possible from such a high sequence homology for the study. TRPC1 also has 4 ARD, 7 HLH, pre-S1 elbow, pre-S1 helix, 6 transmembrane domains, TRP helix, connecting helix and CCD.

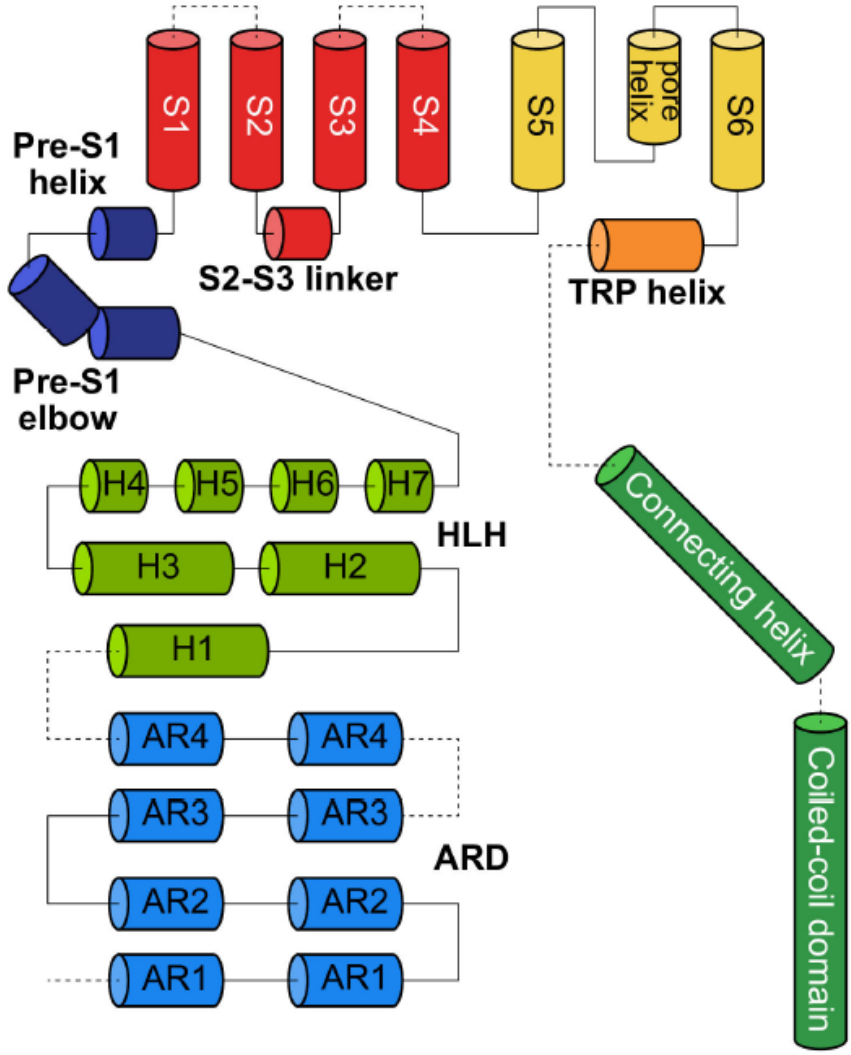


**Figure 2.** Structure of TRPC4 (12). From the N-terminus, ankyrin repeat domain, helix-loop-helix domain, Pre-S1 elbow and helix, voltage sensor like domain (VSLD) (S1-S4), S5, pore-helix, S6, TRP box, connecting helix, coiled-coil domain.

TRPC4 homotetramers form a calcium permeable nonselective cation channel, but it is known to heteromultimerize with other TRPC channels in the subfamily (13). Heteromerization with TRPC1 is a topic of great interest due to TRPC1's ubiquitous expression in the mammalian system, and also because the physiological significance of such modulation is not clearly understood. TRPC4 and TRPC1 share a close homology with each other, as well as in the pore region. Therefore, I decided to focus on the roles of residues that form the narrowest pore.

### TRPC1 as a channel or an ancillary subunit

Although TRPC1 was the first mammalian TRP gene to be cloned, the role of TRPC1 has remained quite elusive among researchers (14). It has been controversial whether TRPC1 constitutes a channel or is merely an ancillary subunit of a channel, but more recent evidences point towards TRPC1 being a channel subunit (15). Despite it being a transmembrane protein, overexpression of TRPC1 alone does not translocate effectively to the plasma membrane (13). Co-immunoprecipitation studies and confocal imaging using fluorescent-tagged proteins showed that TRPC1 only reaches the plasma membrane when co-expressed with TRPC4 or TRPC5 (16). When co-expressed with TRPC3 or TRPC6, the colocalization in the plasma membrane is much lower than the case where TRPC4 or TRPC5 is co-expressed.

Moreover, when TRPC1 by itself was expressed in HEK293 cells for whole cell current measurement, the current sizes were no different from the control transfected cells (15, 17). From these findings it can be concluded that TRPC1 does not seem to be able to form a functional channel on its own, but do heteromerize with other

members of the TRP family to form channels (18). It is speculated that regulation of TRP channels is done through heteromerization with TRPC1, although the area remains largely an unknown area of research.

### The importance of heteromeric channels

Many ion channels are heteromers, meaning that two or more different polypeptides come together to form a functional channel. The physiological significance of heteromers is not well known as of yet, but as different types of proteins are expressed to different extent in various tissue types, heteromerization is thought to be a mode of modulation of ion transport in various tissues depending on the expression pattern. A well-known example of a heteromeric ion channel is the KCNQ2/3 voltage gated potassium channel, where either KCNQ2 or KCNQ3 expressed alone is unable to elicit a meaningful current but when the two heteromerize, the heteromeric ion channel is able to produce a huge current responsible for the M-current crucial in regulation of subthreshold excitability in firing neurons (19). Heteromers are found in TRP channels as well, where PC-1 and PC-2 polypeptides form a polycystin complex well known for its mutation in the pathogenesis of autosomal dominant polycystic kidney disease (ADPKD) (20). Heteromer research is valuable in terms of therapeutic research, since its restrictive tissue expression can be selectively modulated by drugs. By understanding the behaviors of heteromers and their activation mechanism, novel drugs and therapies that target these channels can be more effectively utilized.

The importance of heteromerization is again highlighted as TRPC1 is known to heteromerize with other channels in the TRP

family. TRPC1 heteromerize with TRPP2, and in contrast to either one of the subunits not being able to produce a significant current, the activity is increased 10-fold when the two proteins are expressed together (21). Heteromerization of these proteins may also have a significant role in pathogenesis of ADPKD, as the interaction site between the two molecules, D886 of TRPP2, is also identified as a mutation site in an affected ADPKD family. Therefore, heteromer research is an overlooked but a critical area of research needed for our understanding of the activity of many different channels.

## The TRPC1/4 heteromer complex

Physiological roles of TRPC1/4 heteromers in native tissue have been demonstrated in many studies. In mouse hippocampus, neurons lacking TRPC1, TRPC4, or TRPC5 showed decreased action potential triggered excitatory postsynaptic currents, and mice behavior showed deficiencies in spatial working memory and relearning (22). Astrocytes express TRPC1, TRPC4 and TRPC5, and inhibition of TRPC1 decreases calcium-dependent glutamate release in these cells (23). Moreover, TRPC1/4 heteromer plays a role in epilepsy-induced cytotoxicity and neurodegeneration as shown from knockout studies (24, 25). Not only in neuronal tissues, but TRPC1 and TRPC4 are also involved in corporal smooth muscle cells (26), cardiac cells (27, 28) and pulmonary tissues (29). Evidences from native tissues suggest that TRPC1 is a negative regulator of TRPC4 and TRPC5, one of them being cases of neurodegenerative diseases like Huntington ' s disease and Parkinson' s disease where TRPC1 protected cells from neuronal death by decreasing calcium influx (11). On the other hand,

TRPC1/4 can also mediate $Na^+$ entry and is involved in $Na^+$ mediated cytotoxicity induced by Englerin A in synovial sarcoma cells (30, 31). In this case, TRPC1 is a positive regulator of TRPC4 and TRPC5.

Heteromerization of TRPC1 and TRPC4 as a mode of modulation of channel activity is evidenced in *in vitro* experiments as well, further emphasizing the importance of this biological phenomenon. Calcium sensitive GCaMP6s tagged TRPC4 was used to measure calcium permeability, and cells expressing TRPC1/4 heteromer showed decreased fluorescence and calcium permeability compared to cells expressing only TRPC4 homomeric channels (32). Relative monovalent permeability is also different in heteromeric channels, as TRPC1/4 heteromers show strong-field-strength site with relative permeabilities of $P_{Na}>P_{Li}>P_{Cs}$, whereas TRPC4 homomeric channels show weak-field-strength site with high $P_{Cs}/P_{Na}$ ratio (15, 33).

## The pore region is important in TRPC4 and TRPC1

Because no Cryo-EM structure of TRPC1 is yet available, we sought to identify the key residues in TRPC1 through comparison with TRPC4 in the same TRPC family, which not only share close homology but is able to form a heteromeric channel with TRPC1. Key residues from TRPC4 we selected as starting points were G577, N580, I617, and N621, as taken from the residues identified as closest along the pore axis (34). Amino acid sequence of TRPC4 was aligned with TRPC1 and the following residues were identified as corresponding residues: S600, H603, V642, and H646 (Figure 4). How these residues and the entire pore region directly contribute to the characteristics of a heteromeric channel was

investigated through mutagenesis and electrophysiological studies.

Previous study using TRPC4 mutants to elucidate the effects of these pore lining residues showed that the selectivity filter and lower gate mutants showed a different conductance pattern and sensitivity to G protein mediated mechanisms (35). Single mutants and combination of the mutants G577S, N580H, I617V, N621H has been examined for its effect on the I-V curve. The quadruple mutant shows an almost linear I-V curve when activated with Englerin A, a potent TRPC4 agonist, which was largely different from the double rectifying I-V curve of wild type TRPC4 homomer. However, when GTP$\gamma$S or $G_i^{Q203L}$ mutant was used to constitutively activate the channel via G protein mediated mechanism, the mutant channel could not be activated. Similar results were obtained with the selectivity filter mutant G577S/N580H. The lower gate mutant, on the other hand, showed a significantly different G-V curve compared to wild type TRPC4 when activated with Englerin A, GTP$\gamma$S, or $G_i^{Q203L}$. From these results, it can be assumed that the pore residues are critical residues in producing the double rectifying I-V curve of the TRPC4 channel, and that substitution to corresponding TRPC1 residues are unable to mimic the current characteristics of a heteromer, but rather renders the channel dysfunctional.

As a follow-up procedure, this study focused on major characteristics of TRPC1/4 heteromeric channel: the decrease in calcium permeability and the outward rectifying I-V curve. The target residues of the pore region were switched from TRPC4 to TRPC1 and vice versa, and the changes in the major channel characteristics were examined to find the core residues that determine the identity of TRPC1/4 heteromeric channel.

To further investigate the molecular determinants for these

distinctive characteristics of TRPC1/TRPC4, the chimeras TRPC1$^{C4\ pore}$ and TRPC4$^{C1\ pore}$ were used by others for demonstrating that the pore region of TRPC1 is crucial for preserving the TRPC1/4 heteromeric channel's physical properties such as its current amplitude, I-V relationship and $Ca^{2+}$ permeation (36). Moreover, the G-S mutation in the S4-S5 linker of TRPC1 could increase the $Ca^{2+}$ permeation of the TRPC1/4 channel complex (36). The pore region is known to affect the conductance and permeability. In TRPV1, there is a cap domain in 13-lined ground squirrel TRPV1 compared to rat TRPV1 (37). Even such a cap domain reduced single channel conductance. Changing the pore lining amino acids causes the permeability to change (38). Even cation channel becomes an anion channel when the pore lining residues are changed. In K2P channels, the mutations of pore lining amino acids changed voltage dependency of K2P channels as well as conductance and permeability (39-42). Similar phenomenon was observed in TRPM2 channels (43).

The pore radius of TRPC1/4 and TRPC4 according to distance along the pore was modeled using SWISS-MODEL, a protein structure homology-modeling server (Figure 3). Key residues determining the radii of the restricting pore region are indicated for both TRPC4 homomer and TRPC1/4 heteromeric channels (S600/G577, H603/N580, V642/I617, H646/N621) (Figure 4). Pore contour modeled for 2:2 stoichiometry of TRPC1 and TRPC4 showed a narrower pore radius when compared with TRPC4 homomer and TRPC1/4 heteromer (1:3 stoichiometry). We predicted that such changes in pore sizes may be responsible for various electrophysiological characteristics of TRPC4 homomer and TRPC1/4 heteromer.

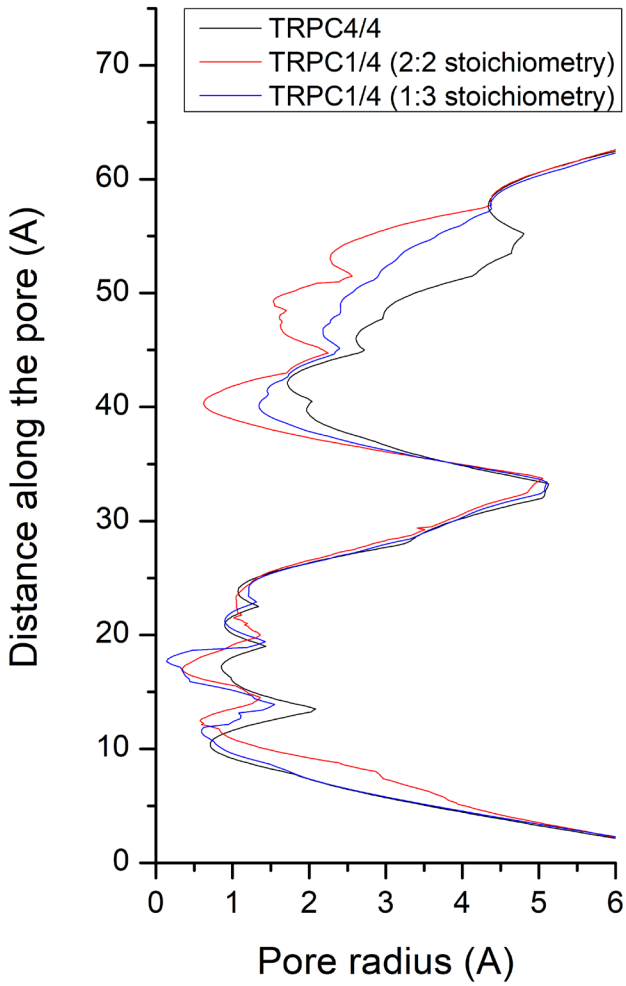


**Figure 3.** Pore contours of TRPC4 homomer and TRPC1/4 heteromers using SWISS-MODEL is illustrated. The greatest difference in distance is observed at the selectivity filter region.

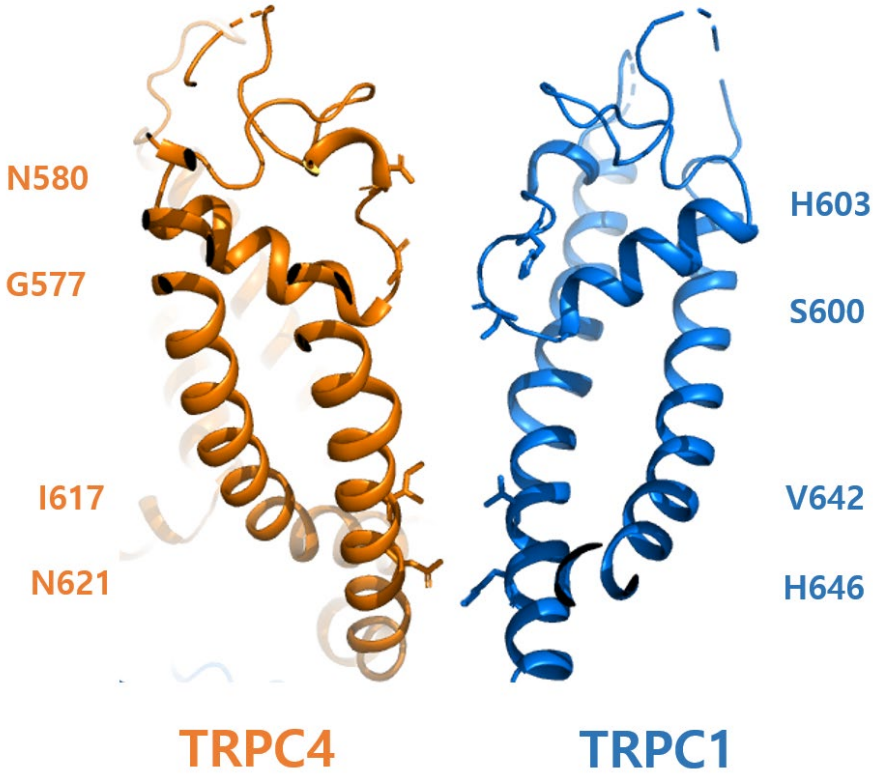


**Figure 4.** Key residues of selectivity filter and lower gate when TRPC1 and TRPC4 are aligned. The residues correspond to the most restricting pore region along the pore axis.

## Current-voltage relationship of TRPC4 and TRPC1/4 channels

The characteristic difference that is most pronounced and most studied between TRPC4 homomeric channel and TRPC1/4 heteromeric channel is the I-V curve. I-V curves of both types of channel is shown, where TRPC4 homomer shows a double rectifying I-V curve with diminished conductance along the membrane potentials of 0 mV to +40 mV whereas TRPC1/4 heteromer shows an outward rectifying I-V curve (Figure 5). Such differences in I-V curve was shown in previous experiments by Strubing et al., where TRPC1 and TRPC4 co-expression in HEK293 cells produced an outward rectifying current (44). When a G-V curve is produced, this difference is clearer as the distinct N-shaped G-V curve of the homomer is not evident anymore in the heteromeric G-V curve (Figure 6, 7). G-V curves were normalized from 0 to 1, 1 being the maximum conductance. In TRPC4 homoteteramer, the conductance increases as the membrane potential depolarized from −120 mV due to intrinsic voltage dependency. From −50 mV, the conductance decreases due to internal cations like $Mg^{2+}$ or spermine. Internal $Mg^{2+}$ binds with D629 near the pore and blocked the outward current physically. From +20 mV to 30 mV, the conductance gradually increases again. In TRPC1/4 heteromer, the conductance increases to the peak. In order to look at how much of the channel property was maintained, the I-V curve shapes were used as a measure of change when looking at the TRPC1 and TRPC4 mutant channels generated later in the study.

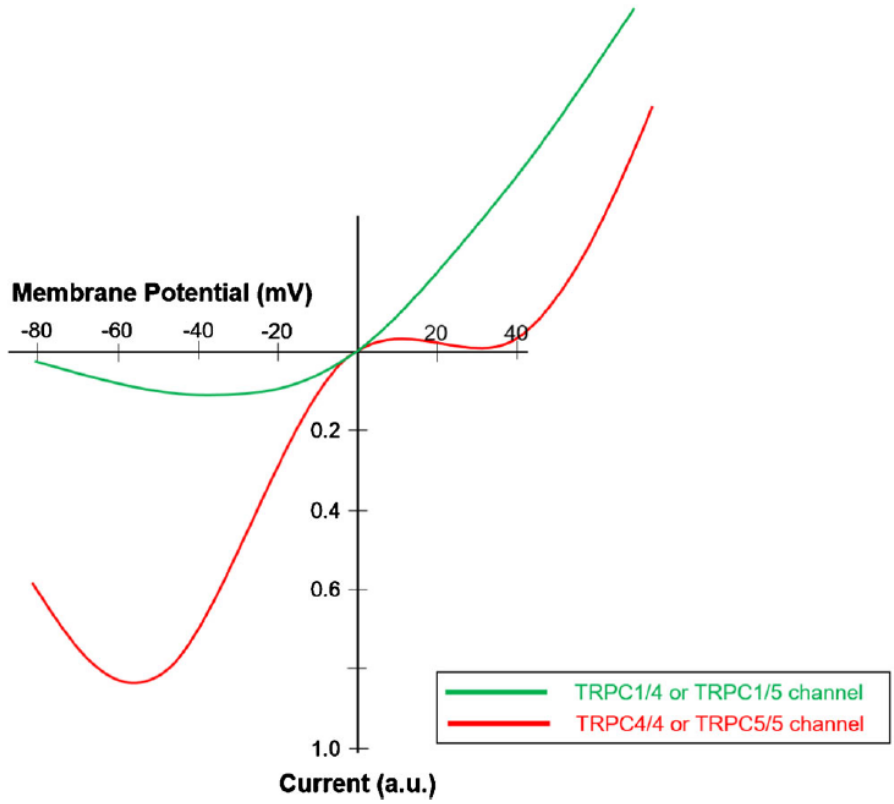


Figure 5. Comparison of the I-V curves of TRPC4 homomeric channel and TRPC1/4 heteromeric channel. TRPC4 homomer shows a double rectifying shape whereas the TRPC1/4 heteromer shows an outward rectifying shape.

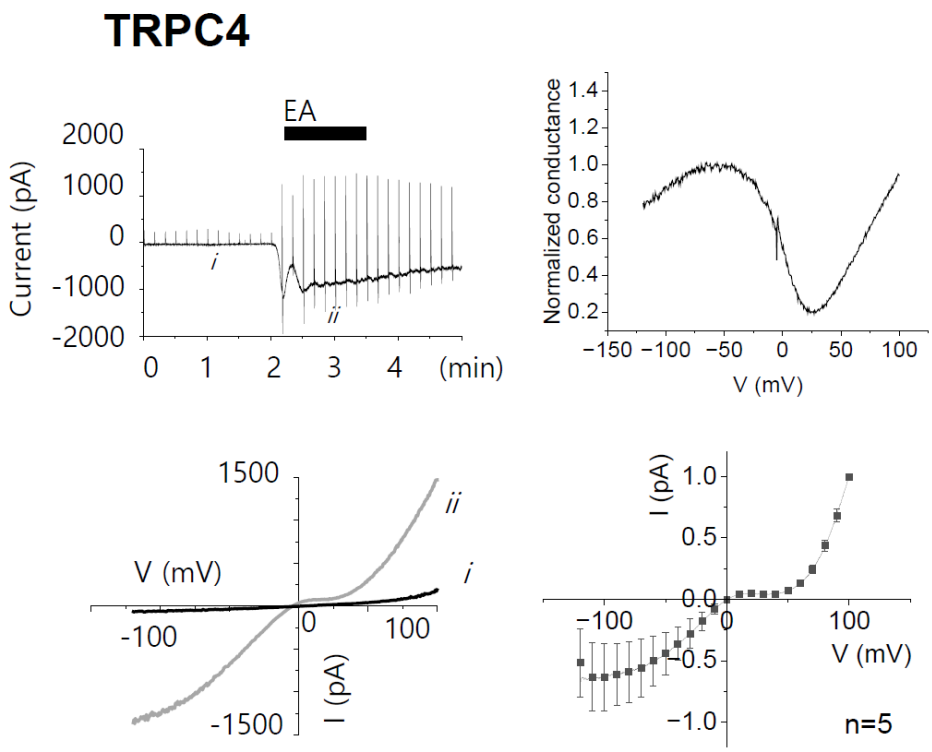


**Figure 6.** Current full trace, G−V curve, and I−V curves of TRPC4. The G−V curve of TRPC4 shows a distinct N−shape.

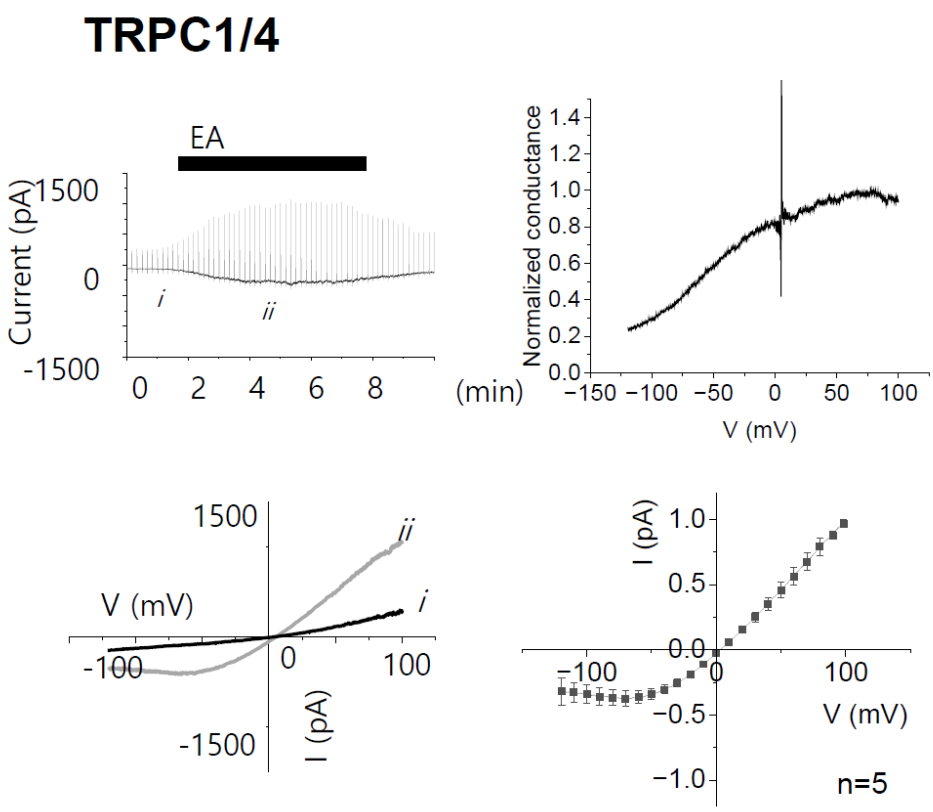


**Figure 7.** Current full trace, G−V curve, and I−V curves of TRPC1/4 heteromer.

# 2. Methods

### Cell culture and transient transfection

Human embryonic kidney cells (HEK293, ATCC, Manassas, VA) were maintained according to the supplier's recommendations. For the transient transfection, the cells were seeded in 12-well plates. In each of the wells, 500 ng of plasmid DNA was transfected using X-tremeGENE$^{TM}$ 9 DNA transfection reagent (Roche Molecular Biochemicals), as detailed in the manufacturer's protocol. After 24-36 hours, the cells were trypsinized and transferred to a recording chamber for whole-cell recording.

### Cloning and Mutagenesis

TRPC1$\alpha$ and TRPC4$\beta$ genes were cloned into pEYFP-C1 and pECFP-N1 vector in our hands, and pEG mCherry-Bacmam vector was kindly donated to us by Dr. Eric Gouaux (Vollum Institute, OR, United States). TRPC4$\beta$-GCamP6s vector was cloned using Gibson Assembly, and all mutagenesis was performed through site-directed mutagenesis using missense primers and PrimeSTAR HS DNA polymerase system (TaKaRa Bio).

### Whole-cell patch clamp experiment

Cells were transferred to a small chamber on the stage of an inverted microscope (TE2000S, Nikon, Japan) and attached to coverslip 10 minutes prior to recording. Glass electrodes with 2.5-3.0 megaohm resistance were used to obtain gigaohm seals. The bath solutions were constantly perfused at a rate of 1-2 mL/min. Currents were recorded using an Axopatch 200B patch clamp amplifier (Axon Instruments, USA). The current was recorded for

500 ms duration ramps from +100 to −120 mV with a holding membrane potential of −60 mV. pCLAMP software v.11 and Digidata 1440A (Axon Instruments) were used for data acquisition and application of the command pulses. Data were analyzed using pCLAMP v.11 and Origin Pro software (Microcal Origin, USA).

### Solution and Drugs

For recording the channels, we used Normal Tyrode and a $Cs^+$−rich external solution. The Normal Tyrode contained 135 mM NaCl, 5 mM KCl, 2 mM $CaCl_2$, 1mM $MgCl_2$, 1 mM glucose and 10 mM HEPES with a pH adjusted to 7.4 using NaOH. The $Cs^+$−rich external solution contained equimolar CsCl instead of NaCl and KCl. When Englerin A was applied, 100 nM of Englerin A solution was made with Normal Tyrode solution. The internal solution contained 140 mM CsCl, 10 mM HEPES, 0.2 mM Tris−guaosine 5' −triphosphate with a pH adjusted to 7.3 with CsOH. We used 0.2 mM guanosine 5' −O−[gamma−thio] triphosphate (GTPγS) for internal solution. For the GCaMP6s experiments, ionophore ionomycin 5 μM in Normal Tyrode was used. All reagents were purchased from Sigma−Aldrich (USA).

### FRET microscopy

HEK293 cells were cultured in a 35 mm coverslip bottom dish. To obtain images and measure FRET efficiency, DV2 dual view system was used with an inverted microscope (100X, oil, Ti Eclipse, Nikon, Japan). CoolLED pE−4000 (UK) was used as the light source. CFP was excited with a 430/24 nm excitation filter (Chroma) and emission light was detected with an optiMOS™ CMOS camera (QImaging, Canada) with an exposure time of 150 ms under the

control of MetaMorph 7.6 imaging software. In a dual-view emission path, emission filters ET470/24 for CFP and ET535/30 for YFP was used (Chroma), with both channels acquired simultaneously. To obtain the FRET efficiency, following calculation was used

$$\mathrm{FR} = \frac{F_{AD}}{F_A} = \frac{[S_{FRET}(DA) - R_{D1} \cdot S_{CFP}(DA)]}{R_{A1} \cdot [S_{YFP}(DA) - R_{D2} \cdot S_{CFP}(DA)}$$

Where S indicates intensity measurement, and R indicates predetermined constants acquired from measurements of cells expressing only CFP- or YFP-tagged molecules. The effective FRET efficiency was calculated by

$$E_{EFF} = E \times A_b = (FR - 1)[E_{YFP}(440)/E_{CFP}(440)]$$

Where E is the intrinsic FRET efficiency when CFP and YFP molecules are associated with each other, $A_b$ is the fraction of YFP-tagged molecules that are associated with CFP-tagged molecules, and the bracketed term is the ratio of YFP and CFP molar coefficients scaled for the FRET cube excitation filter (45).

## Surface Biotinylation

HEK293 cells were seeded in 6-well plates. After PBS wash, cells were incubated in 0.5 mg/mL sulfo-NHS-LC-biotin (Pierce, USA) in PBS for 30 minutes on ice. Biotin was quenched by 100 mM glycine in PBS. Lysates were prepared in lysis buffer (0.5% Triton X-100, 150mM NaCl, 50mM HEPES, 2mM $MgCl_2$, 2mM EDTA, pH7.4) via passage 10-15 times through a 26-gauge needle. Avidin beads were added to 300 $\mu$g of protein lysates and was incubated for 1 hour at room temperature. Beads were washed three times with 0.5% Triton X-100 in PBS, and proteins were extracted and denatured in sample buffer. Total and surface

samples were loaded onto 8% SDS-PAGE gels and transferred onto a nitrocellulose membrane. Anti-GFP (1:5000) (Invitrogen, USA), Anti-Sodium potassium ATPase) (1:5000) (Sigma-Aldrich, USA), Anti-alpha tubulin (1:3000) (Millipore, USA) was used as primary antibody and anti-rabbit (1:5000), and anti-mouse (1:5000) (Bethyl, USA) was used as secondary antibody. Antibody validation for specificity was performed by the suppliers. Blot data were quantified using ImageJ (National Institutes of Health, USA).

### Statistics

Results are expressed as means±standard deviation. Results were compared using either one-way ANOVA and Tukey's test or Student's t-test. $p<0.05$ or $p<0.01$ were considered statistically significant. Statistical analysis was done with GraphPad Prism 5 software (GraphPad Software, USA).

# 3. Results

## 1. TRPC4 lower gate mutants show decreased calcium conductance compared to wild type

The pore region including the selectivity filter is known to regulate ion permeability or selectivity. Because the main difference between TRPC4 homotetramer and TRPC1/4 heterotetramer is the calcium permeability, I used GCaMP6s tagged construct to directly measure $Ca^{2+}$ permeating through the channels. Calcium permeability in various TRPC4 pore residue mutants were examined using GCaMP6s tagged constructs (Figure 7). Individual TRPC4 single mutants (G577S, N580H, I617V, N621H), along with double mutants of the selectivity filter (G577S and N580H), double mutants of the lower gate (I617V, N621H), and the quadruple mutant (all four residues mutated) containing GCaMP6s was expressed in HEK293 cells for calcium conductance measurement. For the activation of the channels, Englerin A (100 nM), a potent TRPC4 specific agonist was used (46). In the wild type TRPC4, we see an increase in calcium permeability followed by the increase in inward current (Figure 8). Ionophore Ionomycin was used to permeabilize the cell for calcium ions at the end of each experiment to test the sensitivity of GCaMP6s.

The selectivity filter single mutants, G577S and N580H, showed diminished but visible calcium influx when activated with 100 nM Englerin A (Figure 9). In G577S, the calcium increase was similar to wild type. In N580H, the calcium increase was smaller than wild type or G577S. On the other hand, the two lower gate single mutants, I617V and N621H, showed larger inward currents

(black trace) but no increasing calcium influx with channel opening (green trace) (Figure 10). Similarly, the lower gate double mutant, which also formerly showed a large current despite its mutations, did not show calcium influx in the GCaMP6s experiment (Figure 10). These results suggest that the lower gate residues also play a role in ion selectivity, particularly calcium ions. The selectivity filter double mutant and the quadruple mutant initially showed no current upon Englerin A activation, and therefore no calcium influx was observed in the GCaMP6s experiments as well (Figure 11). TRPC heteromeric channels containing TRPC1 are known to reduce calcium permeability (17). According to our data, residues in the pore region, particularly the lower gate, and N580 seems to be important in controlling calcium permeability in these channels (Figure 12). The results are unexpected considering the selectivity filter determines the ion selectivity. Especially, histidine mutation instead of asparagine induces a large conformation change within a narrow pore and decreases calcium permeation.

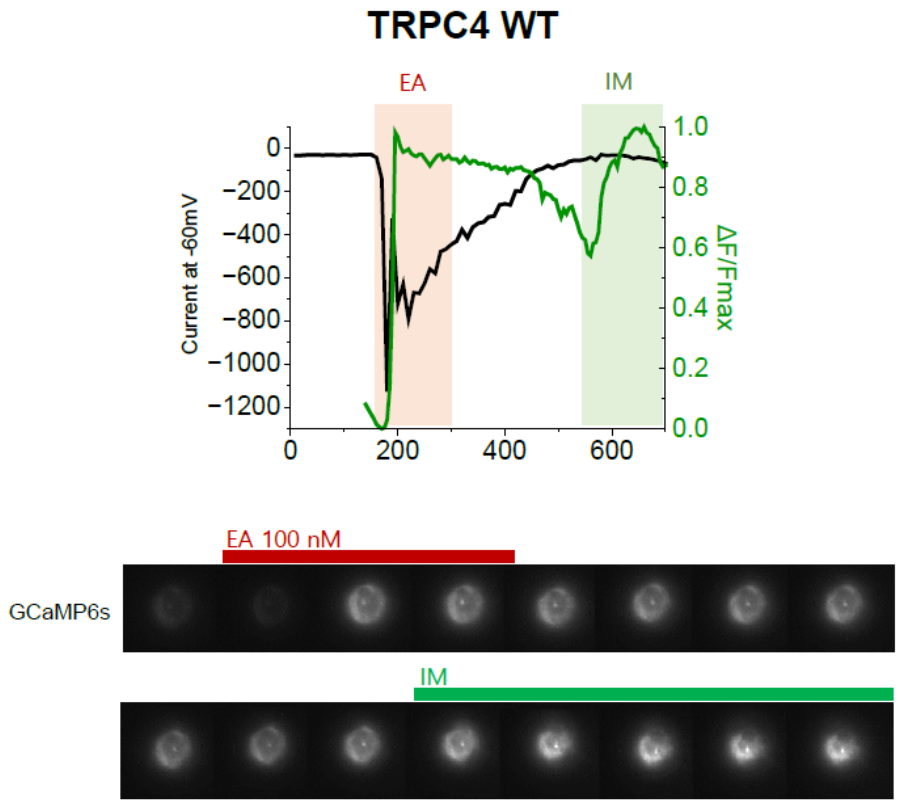


**Figure 8.** Calcium permeability of TRPC4 pore mutants. A. Graphs of inward current at −60 mV and change in $F/F_{max}$ of GCaMP6s fluorescence according to time (sec) is shown for a HEK293 cell expressing wild type TRPC4. Time-lapse snapshots of GCaMP6s fluorescence during one full experiment is shown (40 sec interval). Ionophore Ionomycin was given at the end of the experiment to permeabilize the cell to induce full intensity of GCaMP6s fluorescence.

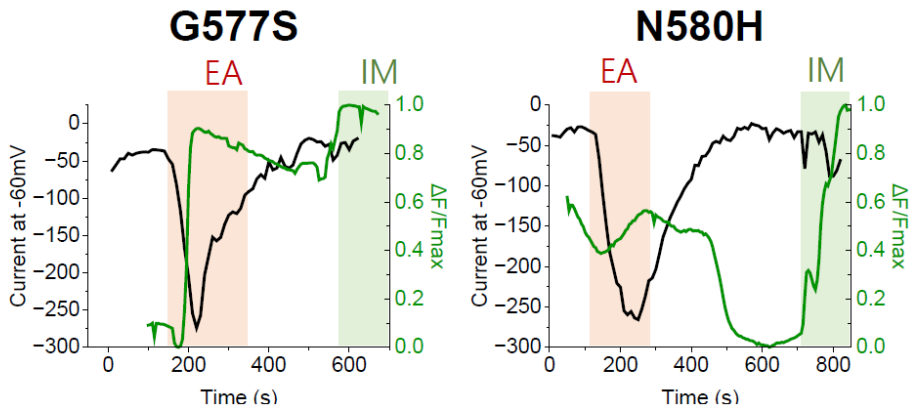


**Figure 9.** Graphs of inward current at −60 mV and change in $F/F_{max}$ of GCaMP6s fluorescence in single mutants of the candidate TRPC4 pore residues. G577S shows robust calcium influx in response to 100 nM Englerin A. N580H shows only minimal calcium influx in response to EA.

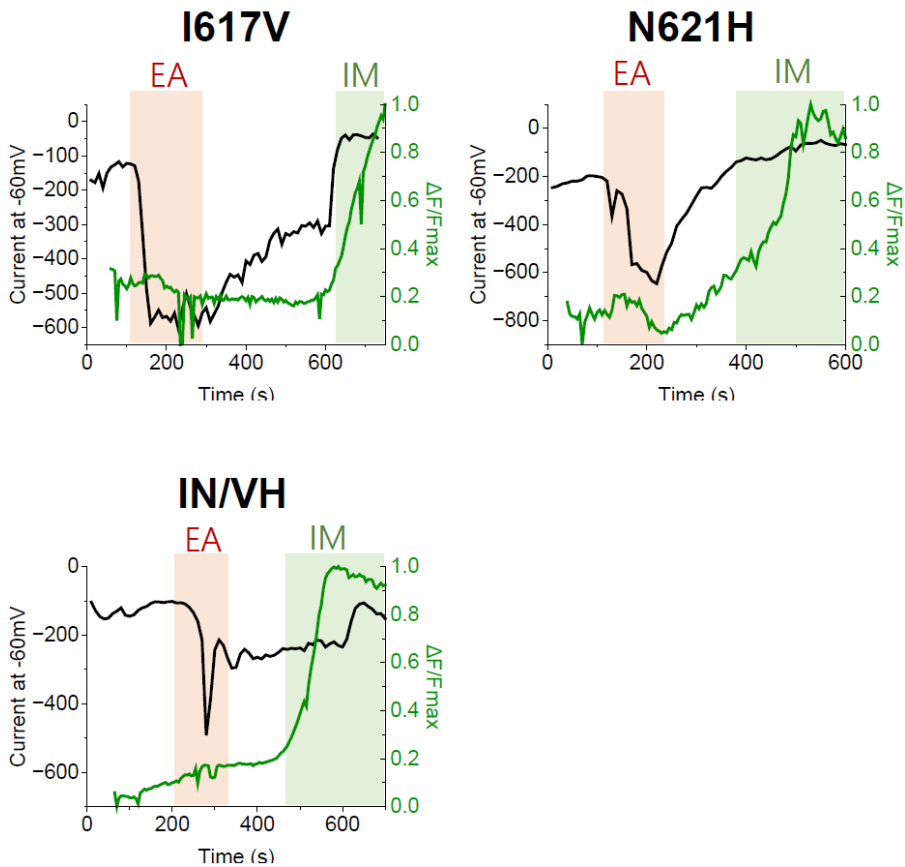


**Figure 10.** Graphs of inward current at −60 mV and change in $F/F_{max}$ of GCaMP6s fluorescence in single and double mutants of the candidate TRPC4 pore residues. I617V, N621H and the lower gate double mutant show no calcium influx upon EA stimulation.

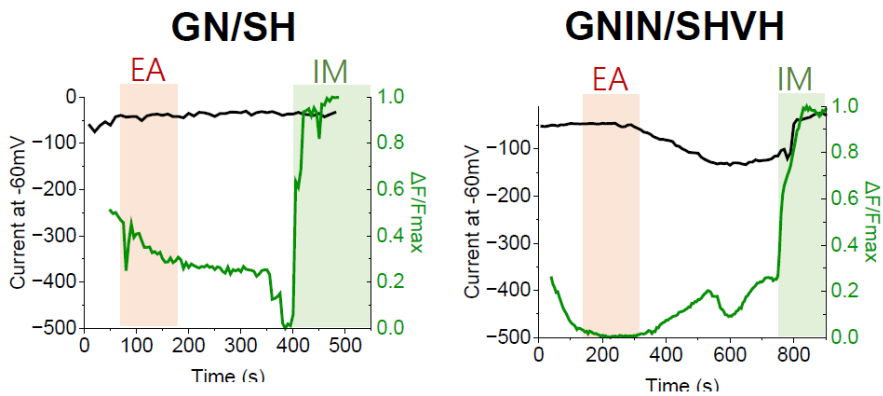


**Figure 11.** Graphs of inward current at −60 mV and change in $F/F_{max}$ of GCaMP6s fluorescence in selectivity filter double mutant and quadruple mutant of the candidate TRPC4 pore residues show no calcium influx upon EA stimulation.

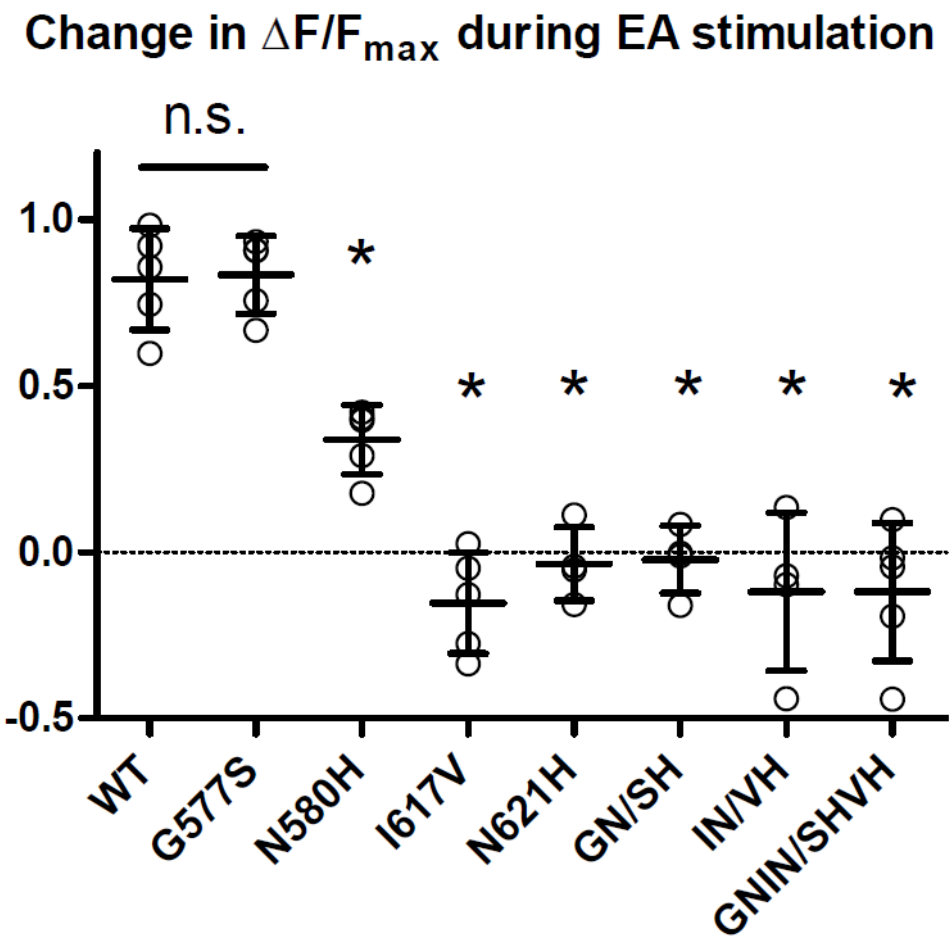


**Figure 12.** Changes in the $\Delta F/F_{max}$ value before and after EA stimulation are compared among mutants (n=5). Normalized mean changes are as follows: 0.82±0.15, 0.83±0.11, 0.33±0.10, −0.15±0.15, −0.03±0.11, −0.02±0.10. −0.12±0.24, −0.12±0.21, for WT, G577S, N580H, I617V, N621H, GN/SH, IN/VH, GNIN, respectively. Data are presented as mean with SD and analyzed using student's *t*−test. *p<0.05

## 2. TRPC4 mutants keep their double rectifying I-V curve shape, but change conductance patterns

In order to see if changing the corresponding residues in TRPC4 is sufficient to affect the I-V curve of a normal TRPC4 current, or in other words, to see if certain residues are important in maintaining the I-V curve of the channel, mutagenesis was done in TRPC4 channels to be compared with wild type (Figure 13). Channels were activated with 100 nM Englerin A. In order to compare the shapes of the G-V curves, slopes A, B and C were calculated from the curve across all mutants (Figure 21). Slope values were calculated using linear fitting procedure based on the highest peak value in the hyperpolarizing range and lowest dip value in the depolarizing range, and the values correspond to the increase in conductance (normalized from 0 to 1) divided by the increase in voltage (in mV). Slope A corresponds to the intrinsic gating of TRPC4, slope B the polyvalent cations (magnesium and spermine) block and slope C the outward current increase at the large depolarizing membrane potential. The single mutants of the selectivity filter, G577s, maintain a double rectifying I-V shape (Figure 14). However, the magnesium block induced plateau is shifted upwards and the resulting change in conductance is shown in Figure 25. Similarly, the single mutant of the selectivity filter, N580H, maintain a double rectifying I-V shape, but the magnesium block induced plateau is shifted upwards (Figure 15, 25). Minimum conductance values from the depolarizing region of the normalized G-V curve has been calculated as well to see the change in conductance patterns (Figure 25). Minimum values of normalized

conductance of wild type heteromer (0.82±0.13), G577S (0.41±0.16), N580H (0.42±0.16) were significantly different from wild type homomer (0.16±0.045) (Figure 25).

The selectivity filter double mutation shows a similar shift in the I-V curve as the single mutants (Figure 16). For slope B, wild type heteromer (0.0026±0.0026), and GN double mutant (-0.0044±0.0048) showed significant difference when compared to wild type homomer (-0.016±0.0035) (Figure 23). The increase in slope B is characteristic of the wild type heteromer, suggesting that the GN double mutant behaves similarly to the wild type heteromer. For slope C, wild type heteromer (0.0014±0.0019), and GN (0.0056±0.0028) showed significant difference when compared to wild type homomer (0.01295±0.0010) (Figure 24). Seeing how the GN double mutant and G577S mutants' slope value decreased suggest that the selectivity filter may be responsible for conductance characteristics in the very depolarizing region. Minimum conductance values of wild type heteromer (0.82±0.13), and GN (0.57±0.12) were significantly different from wild type homomer (0.16±0.045) (*=$p<0.05$, **=$p<0.01$). The selectivity filter mutants' minimum conductance is significantly larger than the wild type homomer at depolarizing potentials, suggesting that the selectivity filter may contribute to the heteromeric channel's behavior in the depolarizing environment.

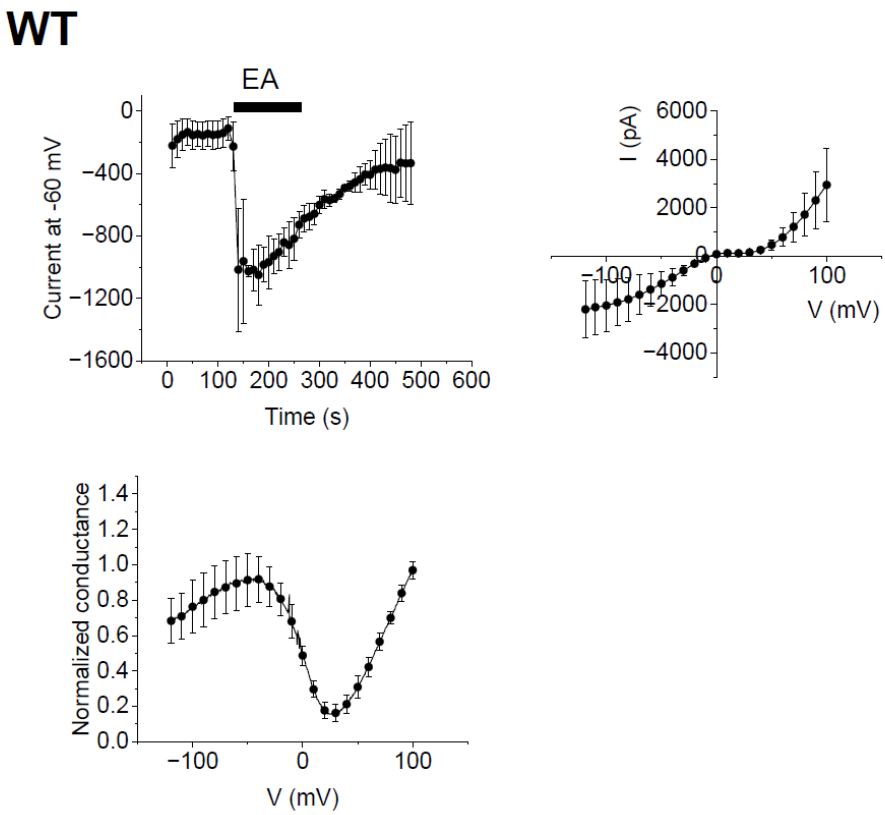


**Figure 13.** Full trace, I−V curve and G−V curve of TRPC4 wild type from whole−cell patch clamp recording. Channels were activated with 100 nM Englerin A. Recordings from 6 to 10 cells were averaged to produce a single curve. For I−V curve and G−V curve analysis, mean and SD were taken every 10 mV interval from −120 mV to +100 mV. All data are presented as mean ± SD. Wild type TRPC4 shows a double rectifying homomeric I−V curve.

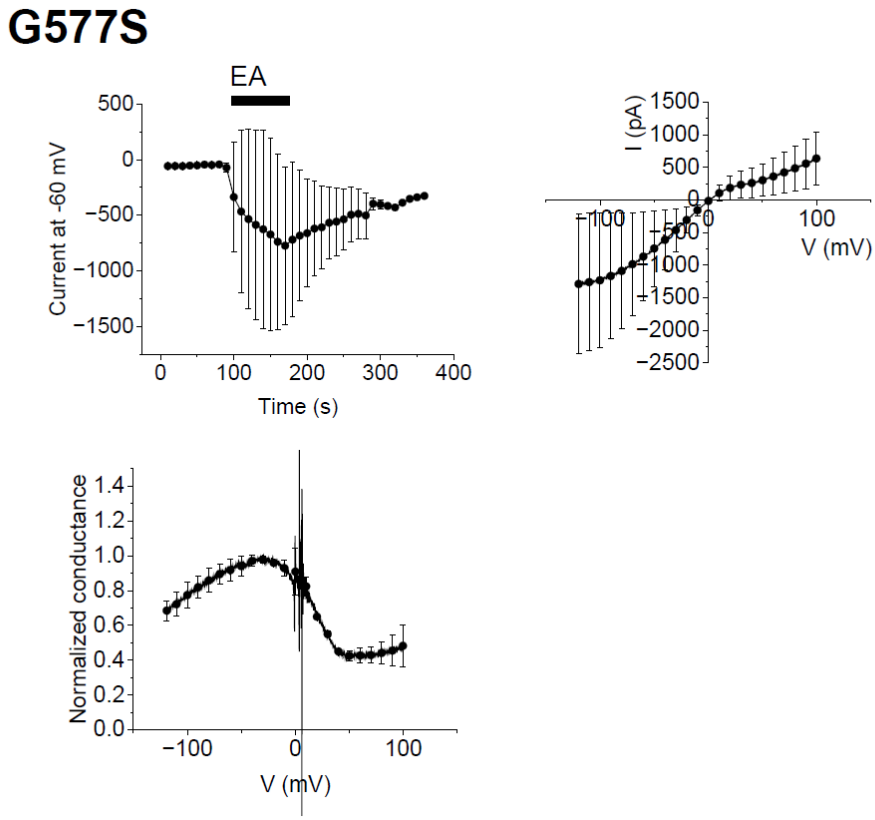


**Figure 14.** Full trace, I-V curves and G-V curves of TRPC4 single mutant G577S from whole-cell patch clamp recording. G577S mutant maintains the double rectifying shape of the I-V curve but shows changes in conductance and a shift in the magnesium block induced plateau.

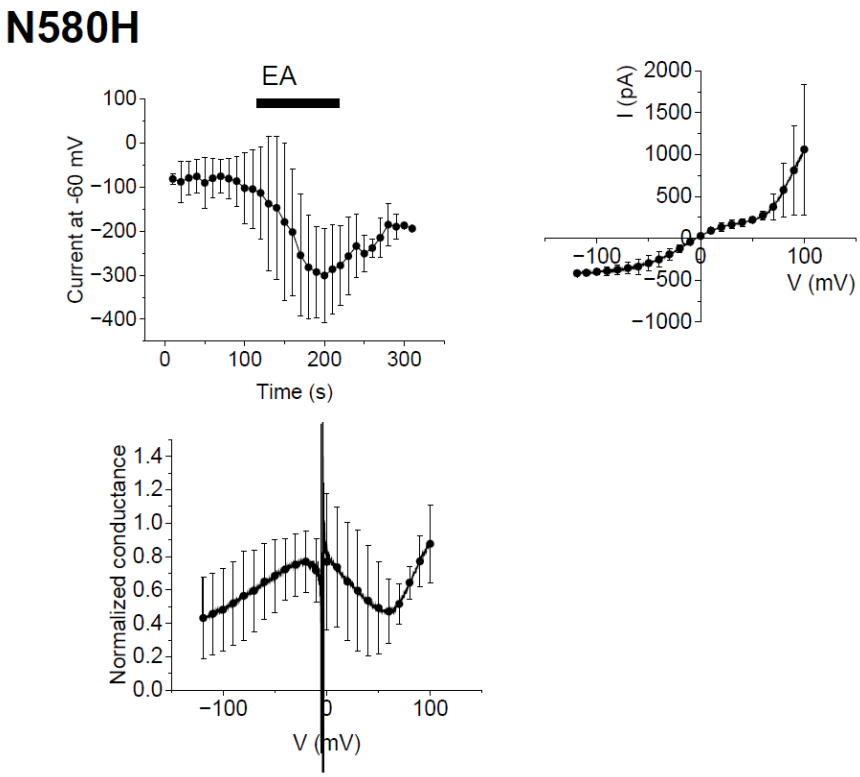


**Figure 15.** Full trace, I−V curves and G−V curves of TRPC4 single mutant N580H from whole−cell patch clamp recording. N580H mutant maintains the double rectifying shape of the I−V curve but shows a shift in the magnesium block induced plateau.

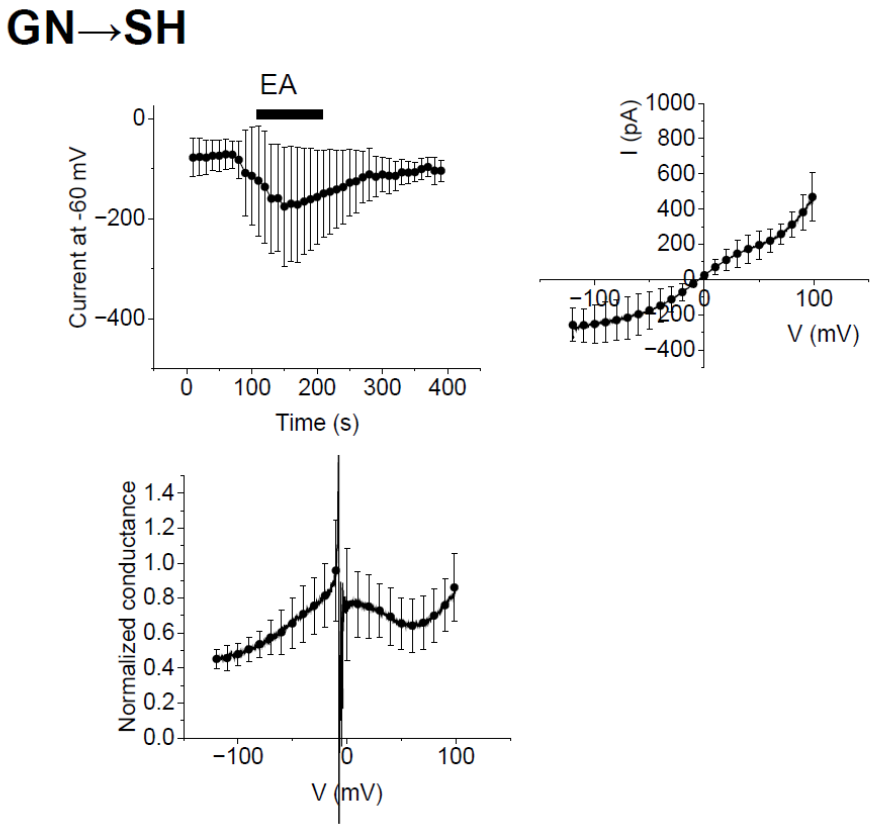


**Figure 16.** Full trace, I−V curves and G−V curves of TRPC4 selectivity filter double mutant GN→SH from whole−cell patch clamp recording. Selectivity filter double mutant maintains the double rectifying shape of the I−V curve but shows a shift in the magnesium block induced plateau as well as change in conductance pattern.

Single mutation at S6 lower gate, I617V, seems to have no effect on the I-V curve of the channel (Figure 17). but the other lower gate mutant, N621H, show a change in the conductance pattern (Figure 18). The lower gate double mutation seems to have no effect on the I-V curve or the current characteristics of the channel (Figure 19). When minimum conductance values from the normalized G-V curve were calculated to see the change in conductance patterns, wild type heteromer ($0.82 \pm 0.13$) and N621H ($0.31 \pm 0.084$) were significantly different from wild type homomer ($0.16 \pm 0.045$) (*=$p<0.05$, **=$p<0.01$) (Figure 25).

When all of the selectivity filter and lower gate residues were mutated in the quadruple mutant, Englerin A-induced current was diminished and only a linear current with constant conductance against the membrane potentials could be observed. (Figure 20). The quadruple mutant GNIN seems not to respond to Englerin A.

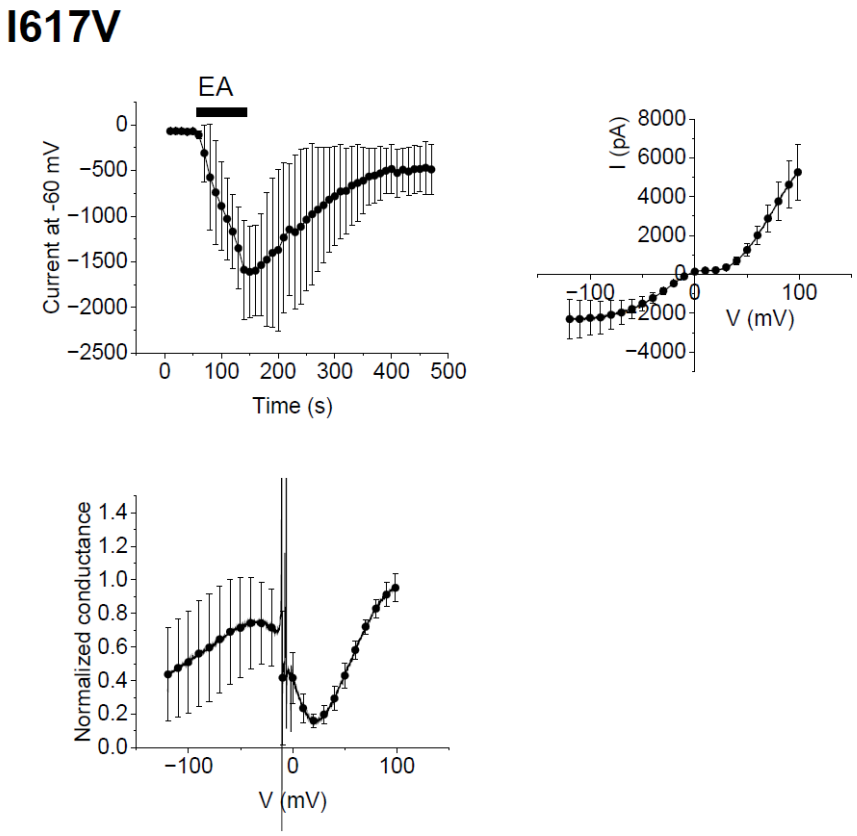


**Figure 17.** Full trace, I-V curves and G-V curves of TRPC4 single mutant I617V from whole-cell patch clamp recording. I617V mutant maintains the double rectifying shape of the I-V curve and N-shaped G-V curves similar to that of the WT.

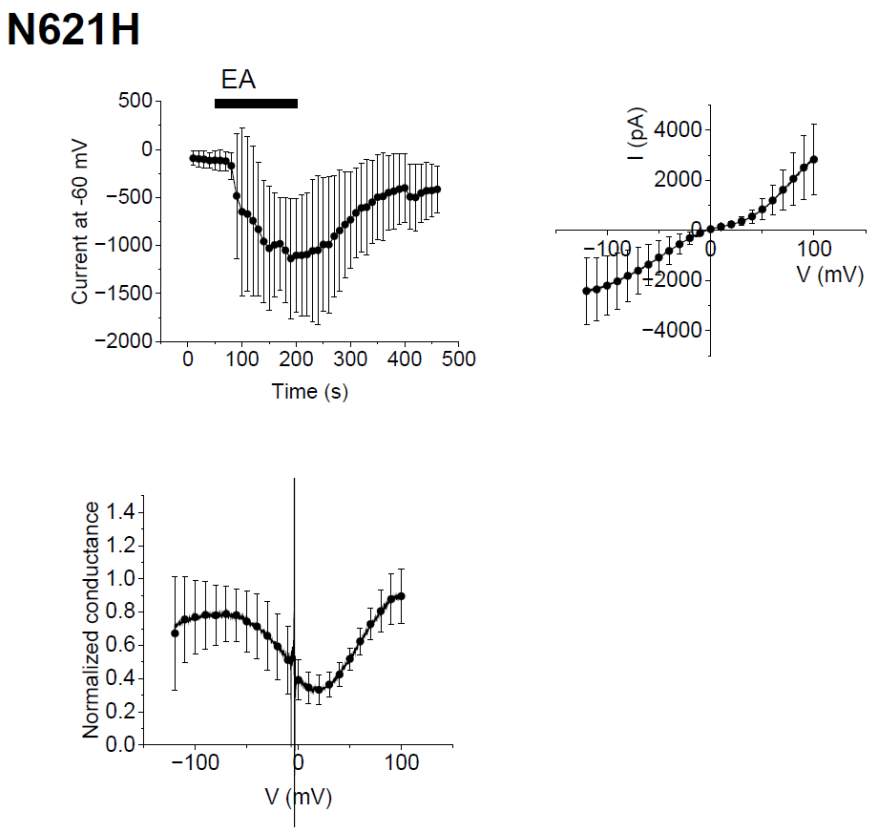


**Figure 18.** Full trace, I-V curves and G-V curves of TRPC4 single mutant N621H from whole-cell patch clamp recording. N621H mutant maintains the double rectifying shape of the I-V curve and N-shaped G-V curves similar to that of the WT.

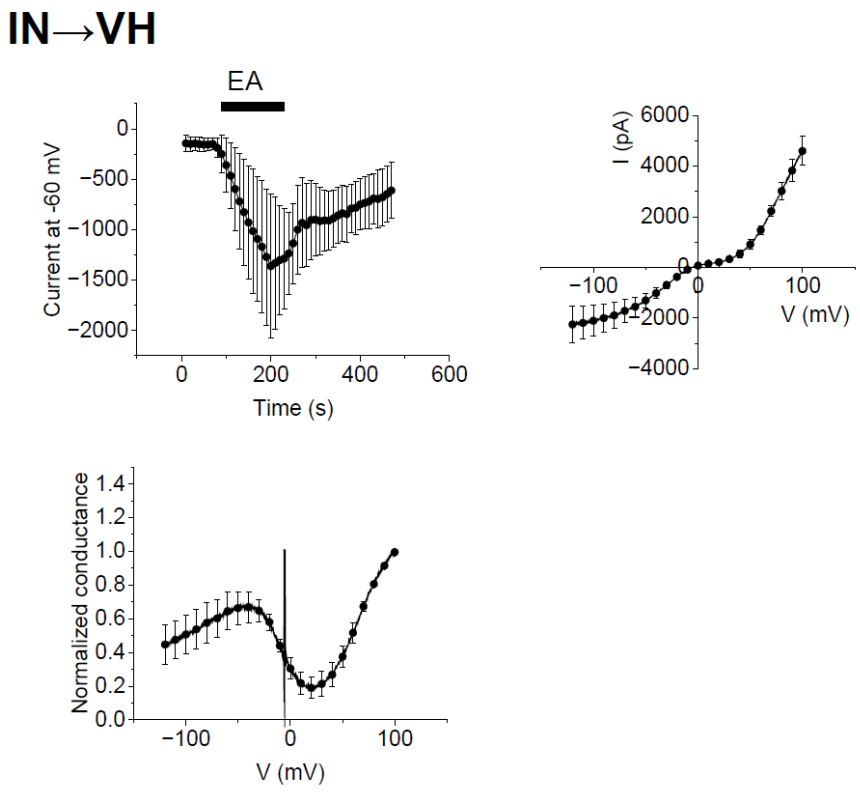


**Figure 19.** Full trace, I−V curves and G−V curves of TRPC4 lower gate double mutant IN→VH from whole−cell patch clamp recording. Lower gate double mutant maintains the double rectifying shape of the I−V curve and N−shaped G−V curves similar to that of the WT.

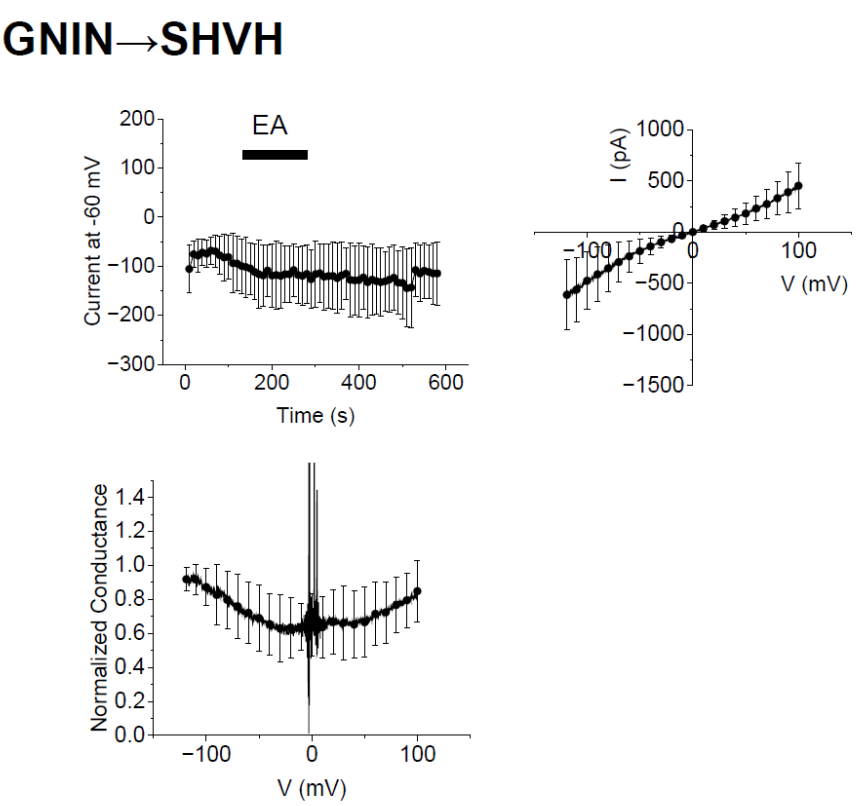


**Figure 20.** Full trace, I-V curves and G-V curves of TRPC4 quadruple mutant GNIN→SHVH from whole-cell patch clamp recording. When all of the selectivity filter and lower gate residues were mutated in the quadruple mutant, Englerin A-induced current was diminished and only a linear current with constant conductance against the membrane potentials could be observed.

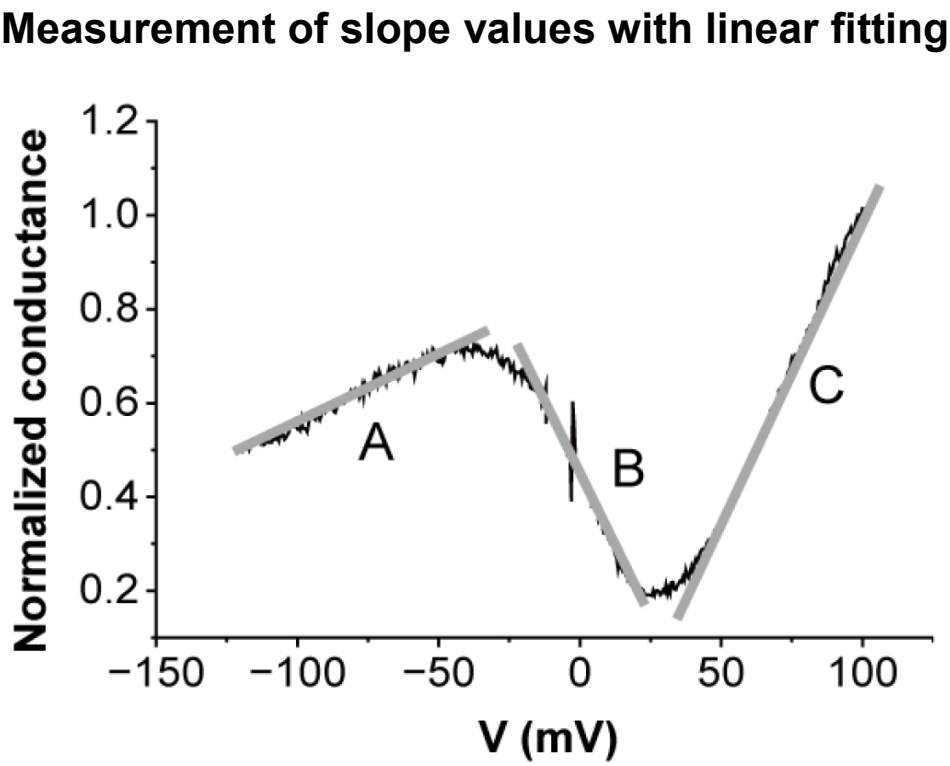


Figure 21. Slope values of A, B and C were calculated from the G−V curves of the mutants. Linear fitting was done for each segment of the N−shaped curve, with the boundaries of the segments determined by the maximum peak and the minimum dip of the curve.

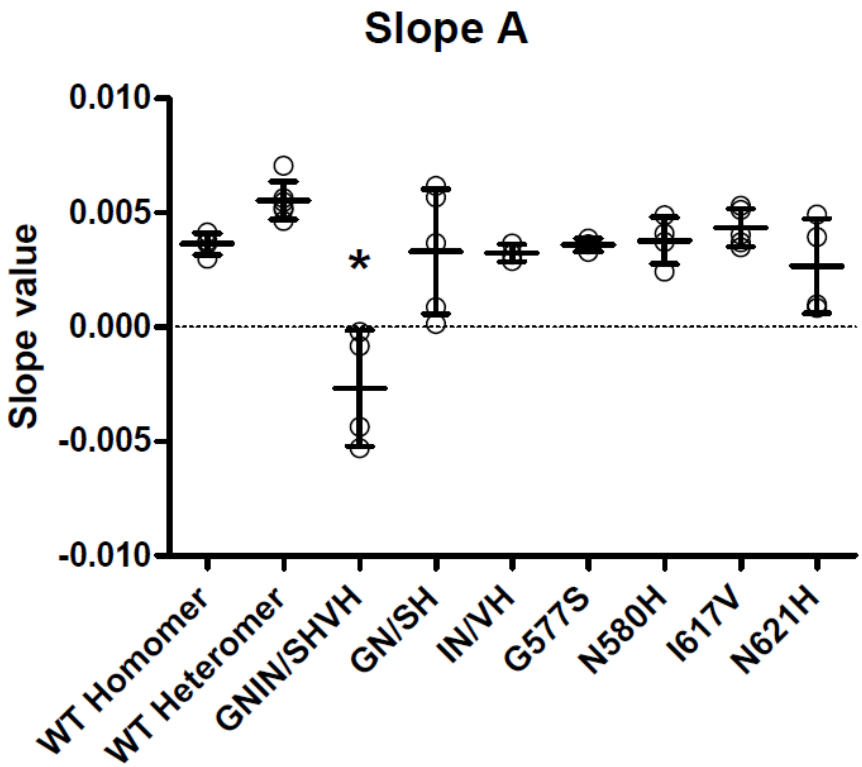


Figure 22. Comparison of the slope value A from wild type homomer, heteromer and the mutants. The quadruple mutant shows a significant decrease in slope value A compared to wild type. Data are presented as mean with SD and analyzed using one-way ANOVA and Tukey's test. *$p<0.05$.

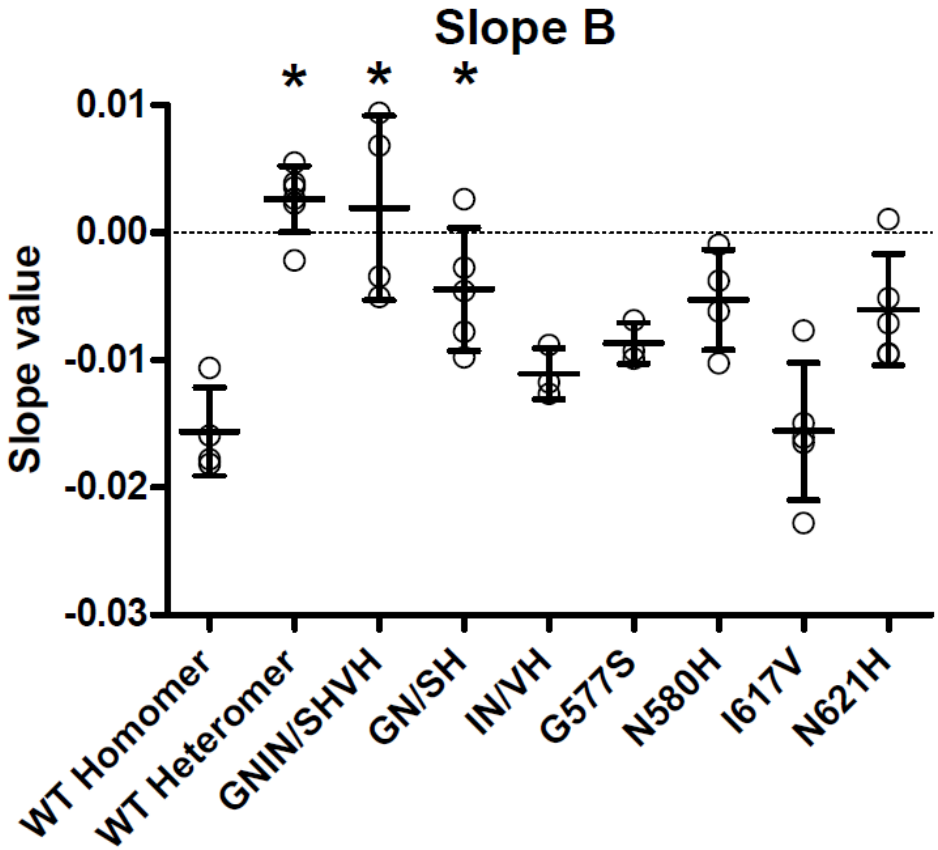


Figure 23. Comparison of the slope value B from wild type homomer, heteromer and the mutants. The wild type heteromer, quadruple mutant, and the selectivity filter double mutant shows a significant increase in slope B compared to wild type.

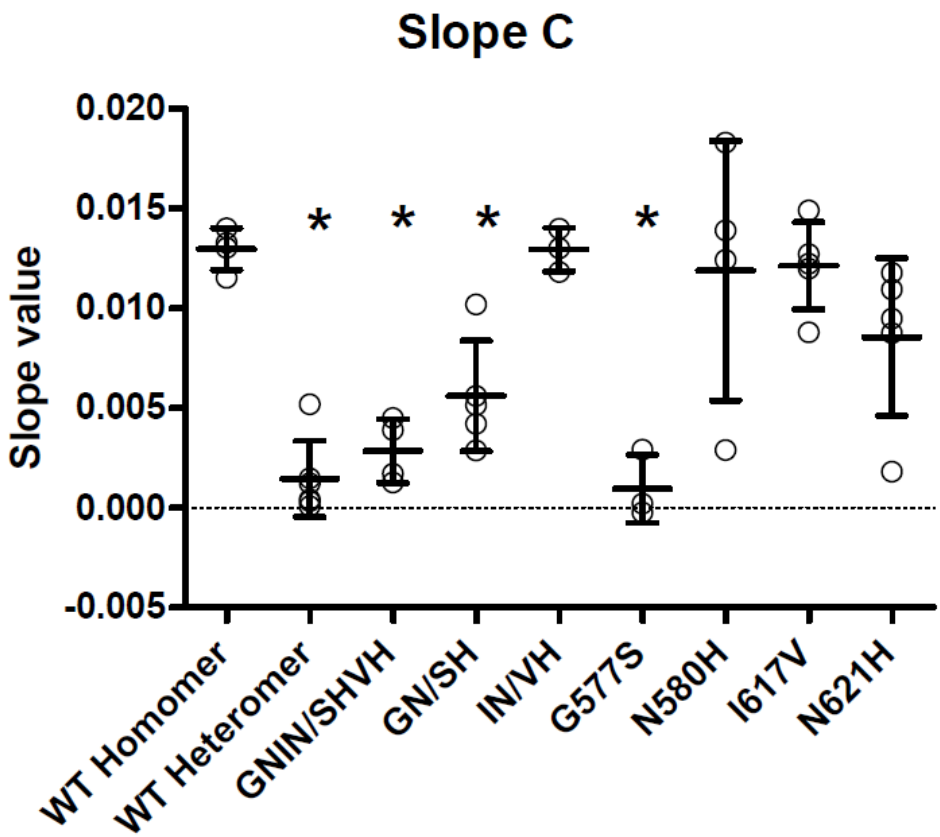


**Figure 24.** Comparison of the slope value C from wild type homomer, heteromer and the mutants. The wild type heteromer, quadruple mutant, and the selectivity filter double mutant and G577S mutant shows a significant decrease in slope C compared to wild type.

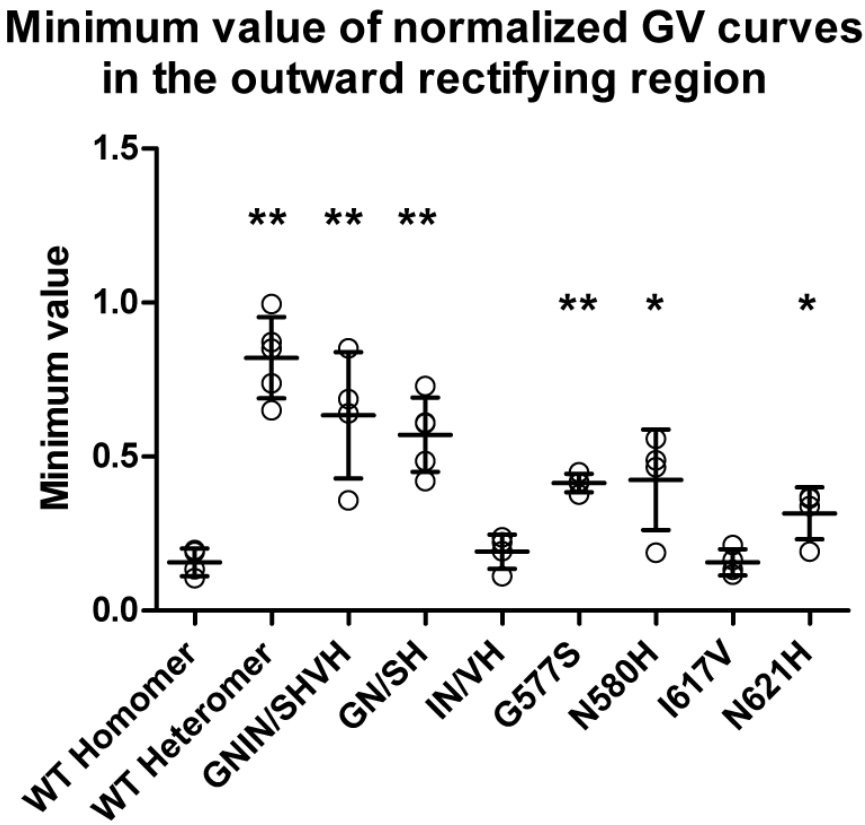


Figure 25. Minimum values of normalized GV curves in the outward rectifying region has been plotted. The selectivity filter mutants show increased minimum conductance values compared to wild type TRPC4 homomer. Data are presented as mean with SD and analyzed using student's *t*-test. *p<0.05, **p<0.01

## 3. TRPC1 single mutants of the pore region maintain the heteromeric outward rectifying I-V curve

After looking at TRPC4 mutants and their characteristics, we shifted the focus to TRPC1 mutants. The single mutant TRPC1 channels co-expressed with TRPC4 showed heteromeric TRPC1/4 current with an outward rectifying I-V curve. Figures 26 through 29 describes each mutant's response along with its conductance curve. The single mutants are not sufficient to change the heteromeric I-V curve into a double rectifying TRPC4 I-V curve.

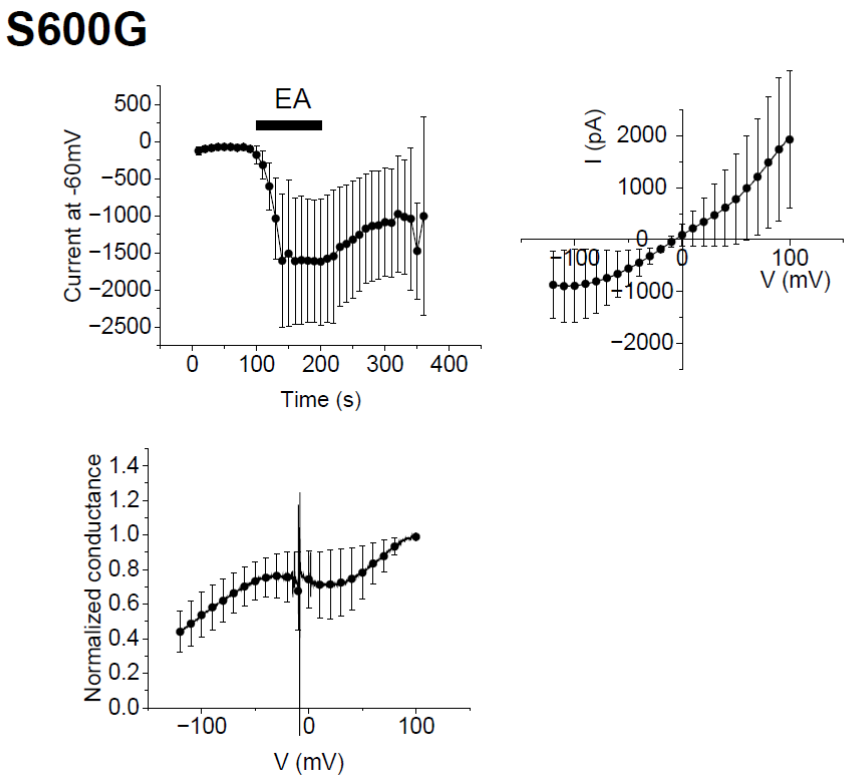


**Figure 26.** Full trace, I−V curve and G−V curves of TRPC1 S600G mutant co−expressed with wild type TRPC4 from whole−cell patch clamp recording. The single mutation is not sufficient to change the outward rectifying shape of the heteromer I−V curve. Channels were activated with 100 nM Englerin A. Recordings from 6 to 10 cells were averaged to produce a single curve. For I−V curve and G−V curve analysis, mean and SD were taken every 10 mV interval from −120 mV to +100 mV. All data are presented as mean ± SD.

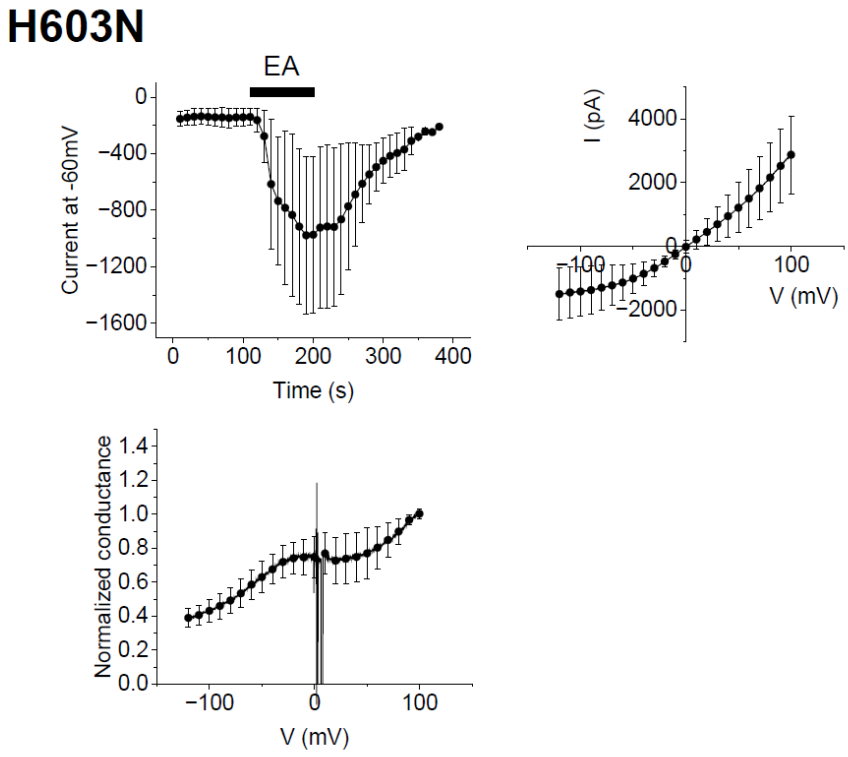


**Figure 27.** Full trace, I-V curve and G-V curves of TRPC1 H603N mutant co-expressed with wild type TRPC4 from whole-cell patch clamp recording. The single mutation is not sufficient to change the outward rectifying shape of the heteromer I-V curve.

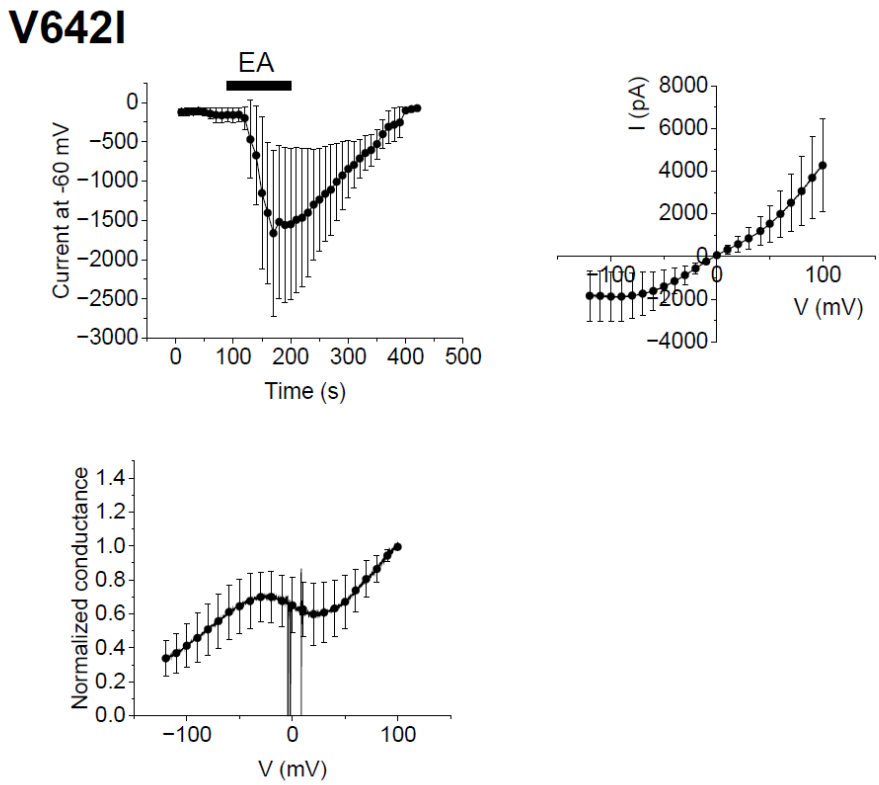


**Figure 28.** Full trace, I-V curve and G-V curves of TRPC1 V642I mutant co-expressed with wild type TRPC4 from whole-cell patch clamp recording. The single mutation is not sufficient to change the outward rectifying shape of the heteromer I-V curve.

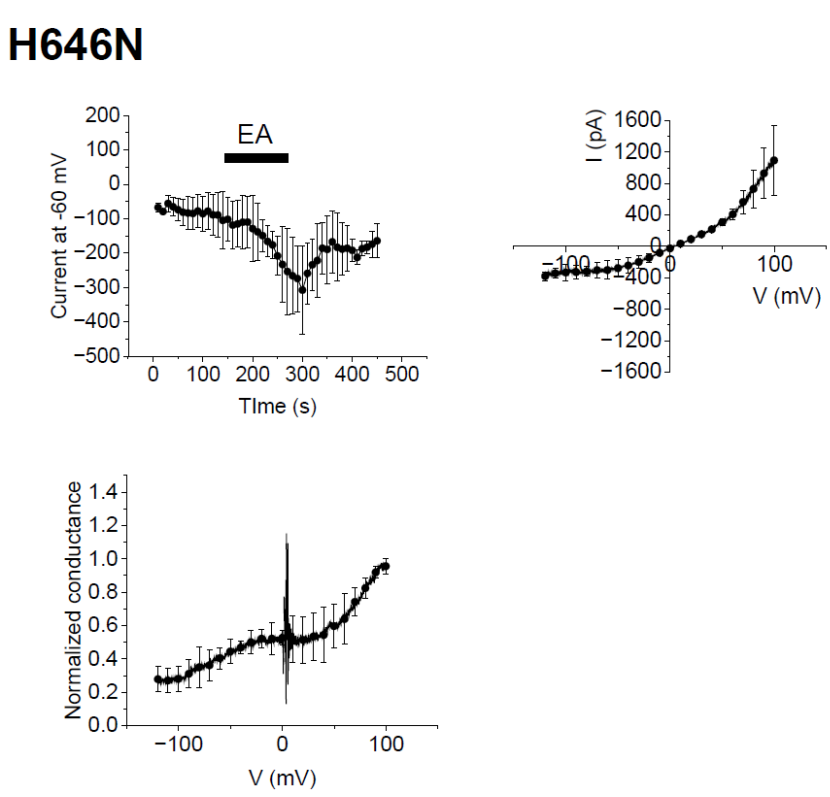


**Figure 29.** Full trace, I−V curve and G−V curves of TRPC1 H646N mutant co−expressed with wild type TRPC4 from whole−cell patch clamp recording. The single mutation is not sufficient to change the outward rectifying shape of the heteromer I−V curve.

## 4. TRPC1$^{C4\ pore}$ chimeras form heteromeric complexes with wild type TRPC4 at the cell membrane

Since the TRPC1 single mutants were unable to change the I-V curve or the G-V curve of the heteromeric channel, chimeric channels of the pore region were made to assess the effects of whole regions of the pore instead of single residues. Chimeric TRPC1 channels were made including the whole selectivity filter and the S6 lower gate of TRPC4 (Chimera 1), just omitting the lower gate residues (Chimera 2), including only the selectivity filter region (Chimera 3), and only the residues 600-603 substituted to TRPC4 residues (Chimera 4) (Figure 30).

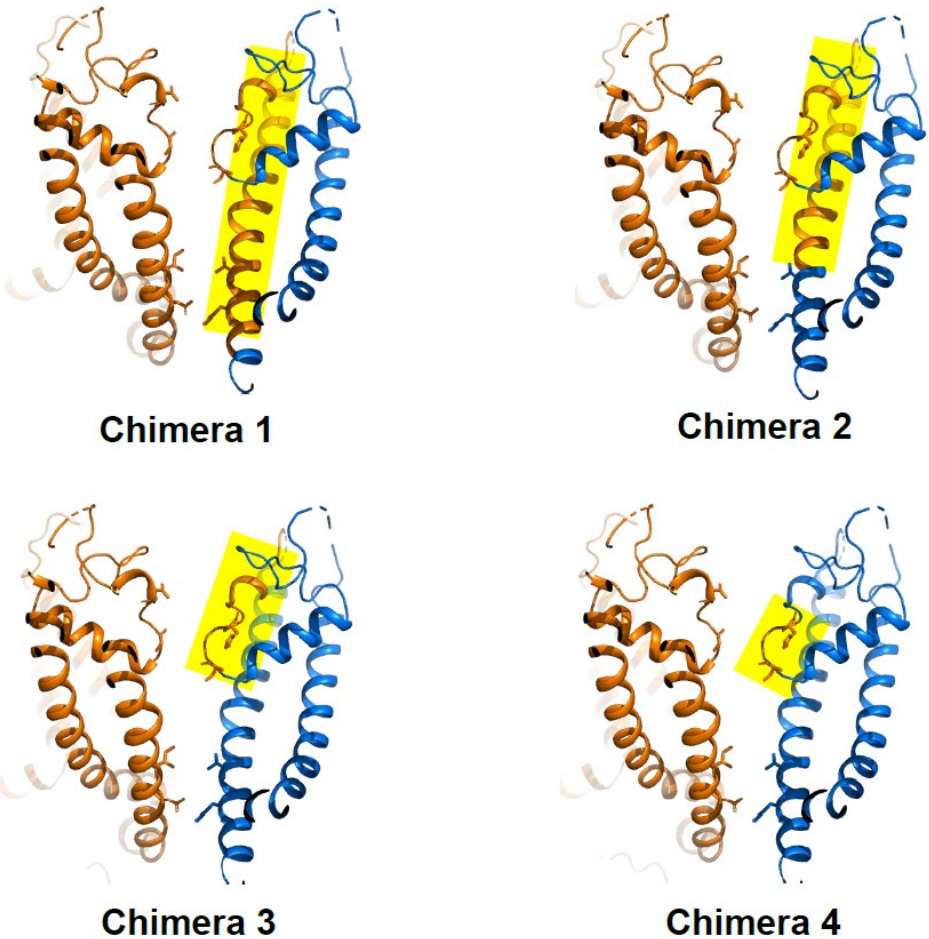


**Figure 30.** Candidate residues are divided into selectivity filter residues and lower gate residues. Chimeric channels were made including the whole selectivity filter and the S6 lower gate (chimera 1), just omitting the lower gate residues (chimera 2), just including the selectivity filter region (chimera 3), and only the four amino acid residues at the selectivity filter (chimera 4).

CFP-tagged TRPC4 and YFP-tagged TRPC1 chimera constructs were generated to examine interaction between the two molecules. Imaging using fluorescence microscopy showed TRPC4 and TRPC1 to co-localize as punctae at the cell membrane (Figure 31). The FRET efficiencies show that the TRPC1 chimeras, like its wild type (19 ± 6.9%, n=8), form a heteromeric complex with TRPC4 (16 ± 5.6%, n=16, 18 ± 10.0%, n=10, 19 ± 9.9%, n=8, 14 ± 2.6%, n=8 for chimeras 1, 2, 3 and 4, respectively. Reported n equals number of cells.) (Figure 32). CFP and YFP concatemer construct was used as a positive control and CFP and YFP expressed in separate constructs was used as a negative control for FRET measurements. Surface biotinylation data shows that the surface expression of TRPC1 chimeras are unchanged regardless of co-expression with TRPC4 (Figures 33, 34). But the blot results indicate surface expression of TRPC1 chimeras in the membrane and together with the FRET data, we can conclude that TRPC1 chimeras and TRPC4 form a heteromeric complex at the membrane surface, as it is with wild type TRPC1 and TRPC4.

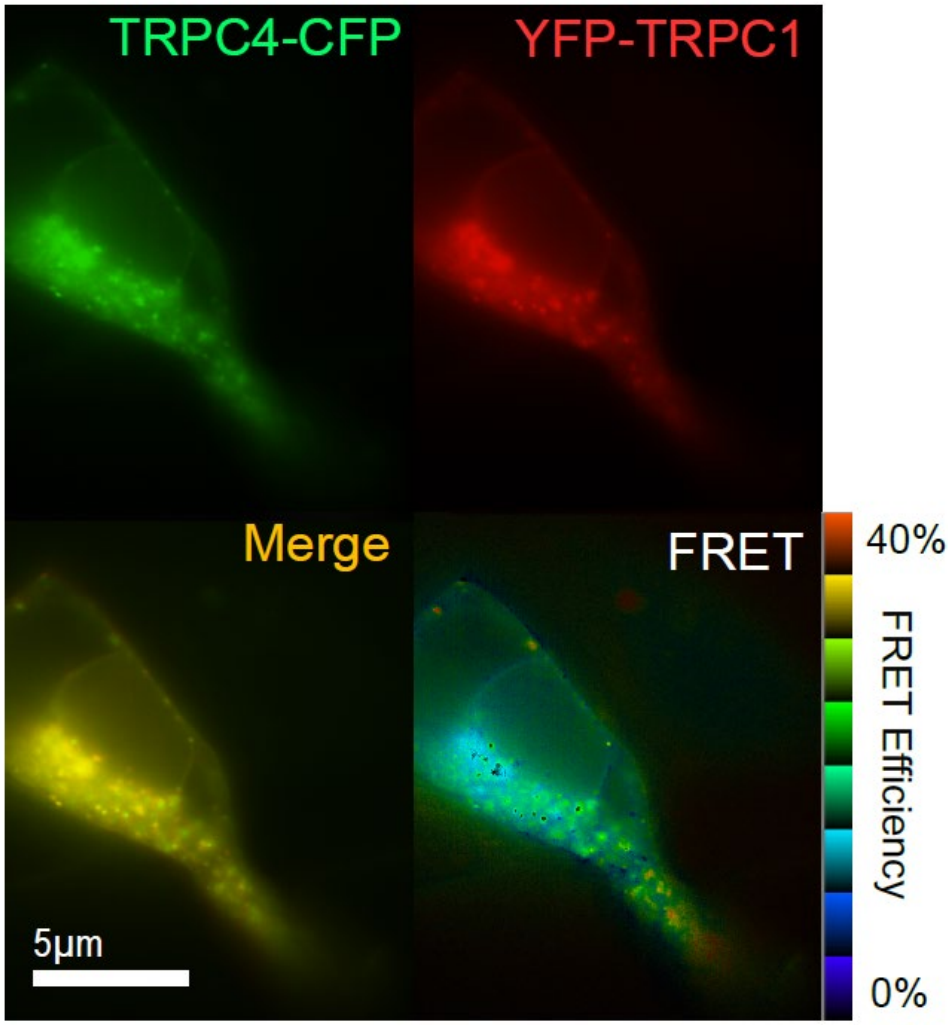


**Figure 31.** Representative image of HEK293 cell co-expressing fluorescent-tagged TRPC4 and TRPC1 chimera. TRPC4 (CFP) and TRPC1 chimera 1 (YFP) are co-localized at the cell membrane as punctae.

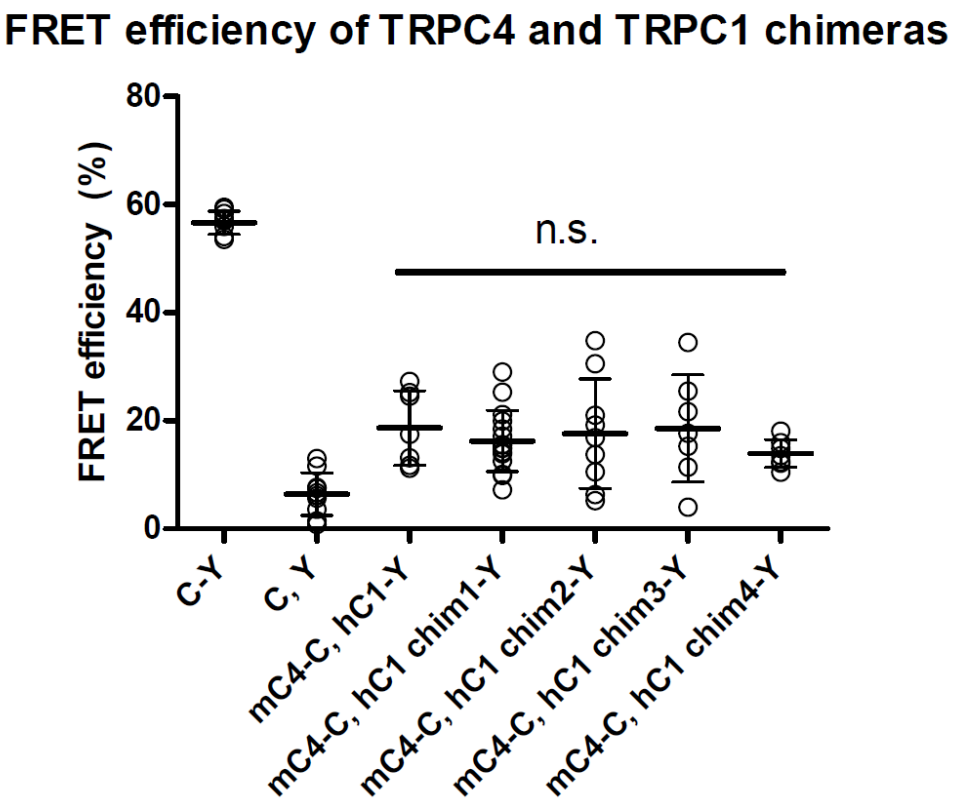


**Figure 32.** FRET efficiencies of fluorescent-tagged TRPC4 and TRPC1 chimeras show that they form a heteromeric complex (n= 8 to 16). TRPC4-CFP coexpressed with YFP-TRPC1 was used as a positive control for FRET. CFP and YFP co-expressed as separate constructs was used as a negative control. The chimeras and the wild type show no significant difference. Data are presented as mean with SD and were analyzed using student's t-test.

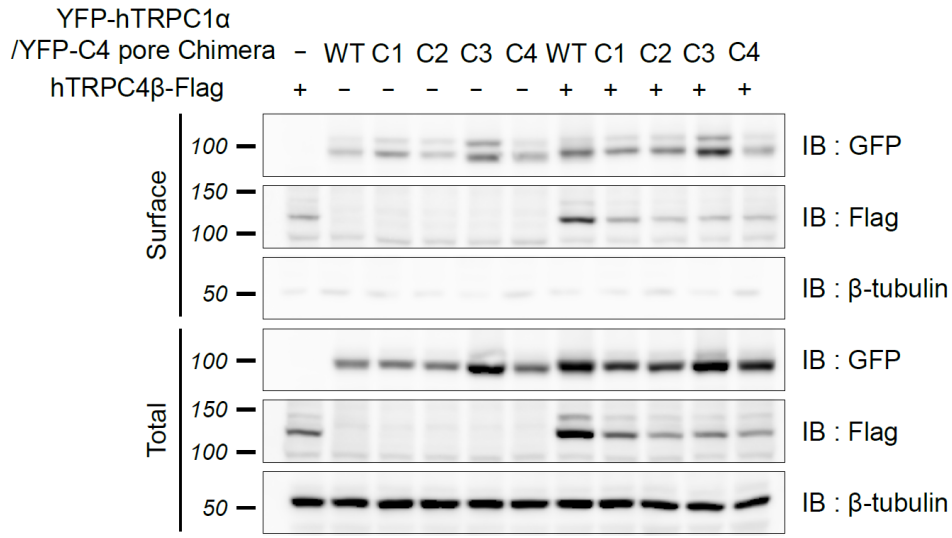


**Figure 33.** Surface biotinylation analysis of TRPC1 chimeras and wild type TRPC4. Regardless of co-expression with wild type TRPC4, TRPC1 chimeras, along with wild type TRPC1 are found at the cell membrane of HEK293 cells.

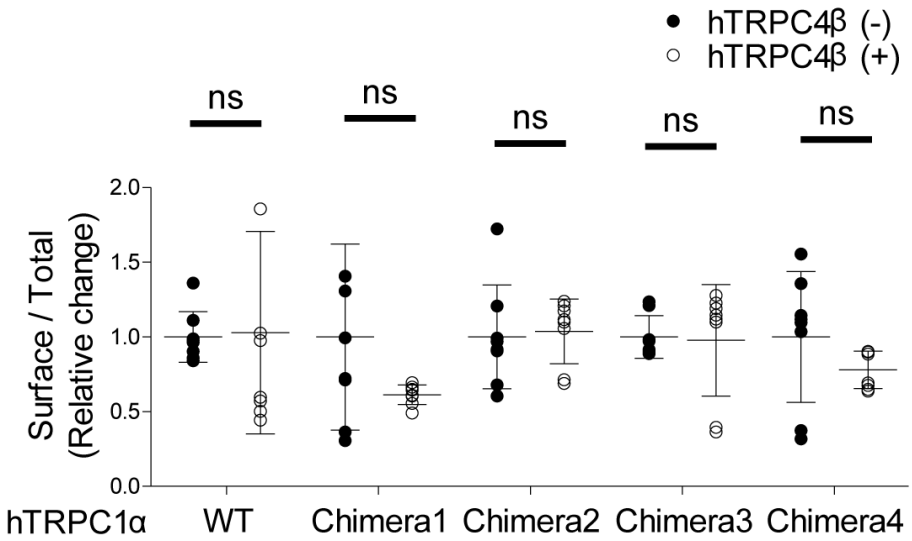


**Figure 34.** Ratios of surface to total amount of protein is non-significant in either TRPC4 positive or negative conditions (n=6 independent observations). Data are presented as mean with SD and analyzed using student's *t*-test. *p<0.05

## 5. TRPC1$^{C4\ pore}$ chimeras 1 and 2 show double rectifying I-V curves

After confirming that the generated chimeras are able to form heteromers with the wild type TRPC4, electrophysiological experiments were performed to observe the change in the voltage dependency of the channels. Chimeras 1 and 2, where most of the pore region is substituted to that of TRPC4, showed a double rectifying I-V curve shape and G-V curves similar to that of a wild type TRPC4 homomer (Figure 35, 36). However, the conductance curve and the I-V curve of chimeras 3 and 4 differ from the other chimeras in terms of shape, indicating that the less similar the pore gets from TRPC4, the more it deviates from the standard double rectifying curve we see in TRPC4 wild type channels (Figure 37, 38).

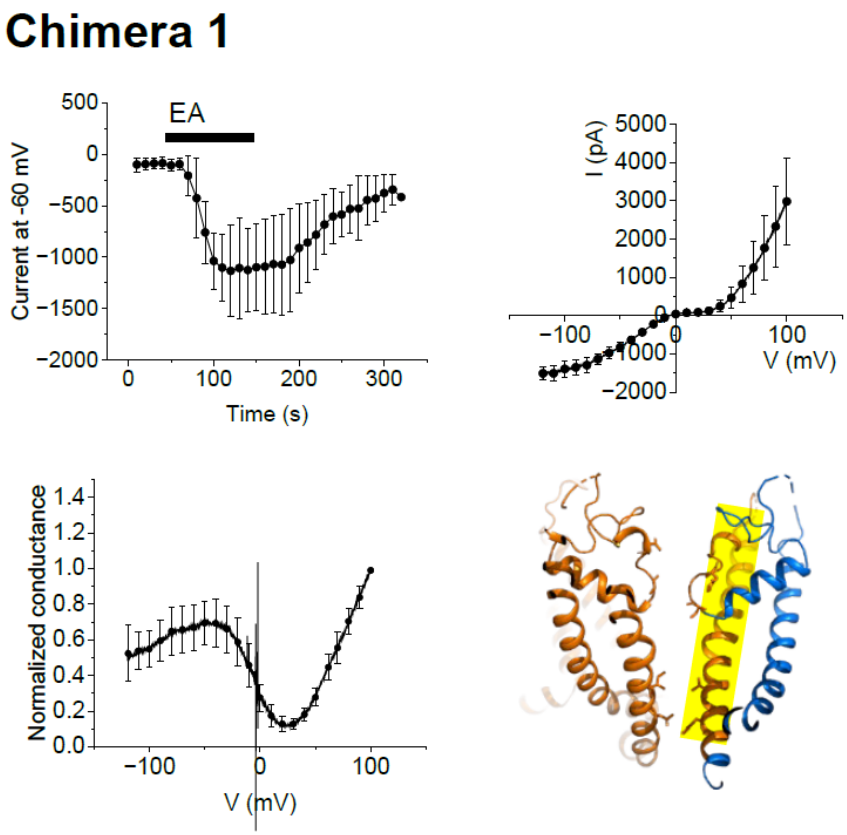


**Figure 35.** Full trace, I-V curve and G-V curves of TRPC1 chimera 1 co-expressed with wild type TRPC4 from whole-cell patch clamp recording. Substituting the pore region of chimera 1 produces a double rectifying I-V curve similar to that of wild type homomer.

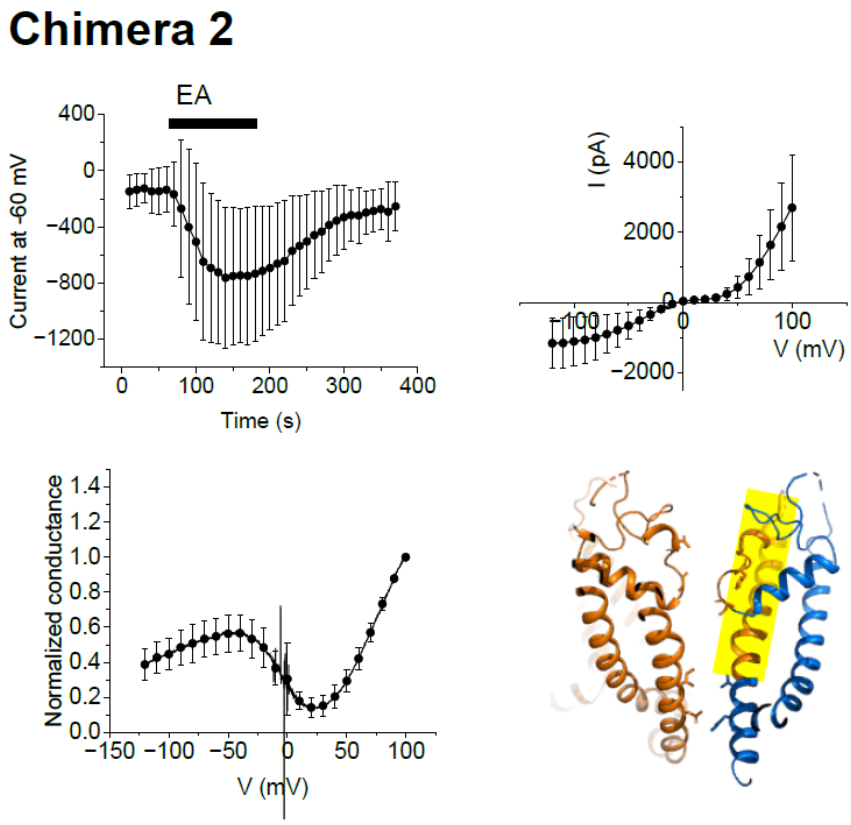


**Figure 36.** Full trace, I-V curve and G-V curves of TRPC1 chimera 2 co-expressed with wild type TRPC4 from whole-cell patch clamp recording. Substituting the pore region of chimera 2 produces a double rectifying I-V curve similar to that of wild type homomer.

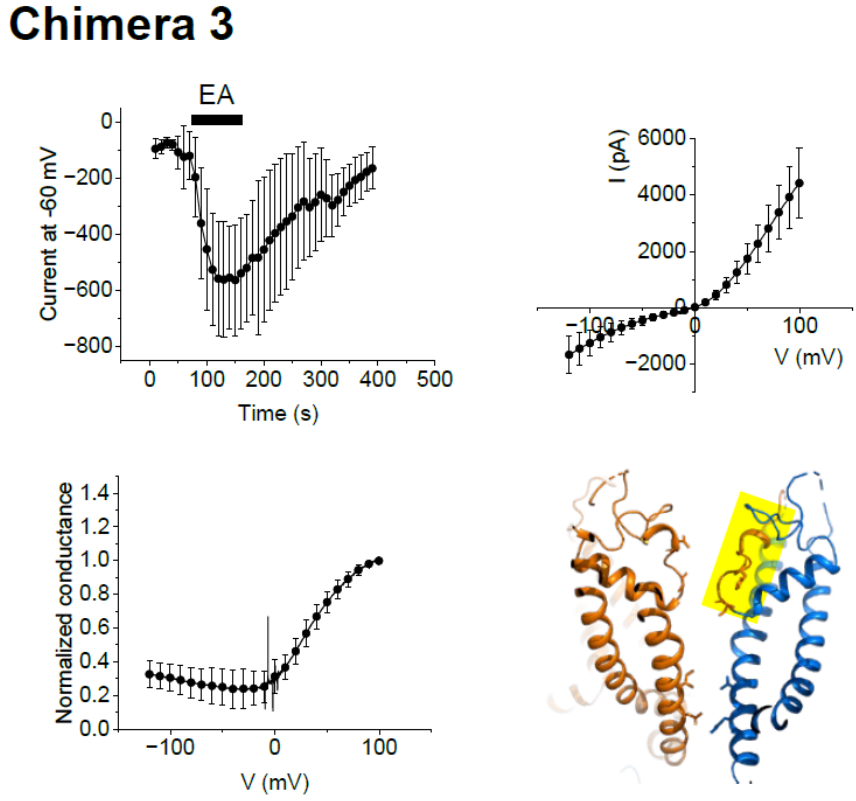


**Figure 37.** Full trace, I-V curve and G-V curves of TRPC1 chimera 3 co-expressed with wild type TRPC4 from whole-cell patch clamp recording. Substituting the pore region of chimera 3 produces an I-V curve shape deviating from the double rectifying shape of wild type homomer, indicating the shift is determined by the regions between chimeras 2 and 3.

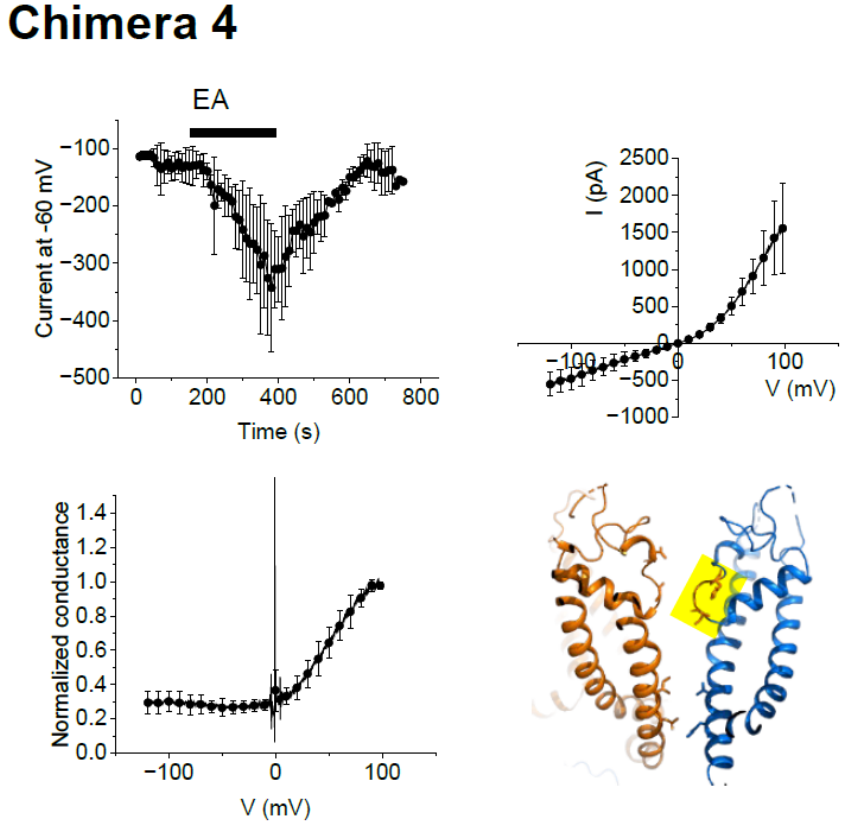


**Figure 38.** Full trace, I-V curve and G-V curves of TRPC1 chimera 4 co-expressed with wild type TRPC4 from whole-cell patch clamp recording. Substituting the pore region of chimera 4 produces an I-V curve shape further deviating from the double rectifying shape of wild type homomer, indicating that as the chimeras get more similar to wild type TRPC1, the more I-V curve loses its double rectifying shape of the wild type homomer.

Slopes A, B, and C were also compared in all G-V curves of the chimeras and mutants. For slope A, chimera 3 (−0.0015±0.00079) and chimera 4 (−0.00049±0.00074) were significantly different from wild type homomer (0.0036±0.00047) (Figure 39). For slope B, wild type heteromer (0.0026±0.0026), chimera 3 (0.0099±0.00074) and chimera 4 (0.0085±0.00042) were significantly different from wild type homomer (−0.016±0.0035), again demonstrating how chimeras 3 and 4 deviate away from the typical N-shaped conductance pattern of a wild type homomer (Figure 40). For slope C, wild type heteromer (0.0014±0.0019), chimera 3 (0.0045±0.0017), chimera 4 (0.0065±0.0030), S600G (0.0046±0.0033), H603N (0.0051±0.0036), V642I (0.0070±0.0035) and H646N (0.0086±0.0026) were significantly different from wild type homomer (0.013±0.0010), indicating that these mutants and chimeras are similar to wild type heteromer in terms of its characteristics (Figure 41). In slope analysis, slope B and C seems to be a good index to distinguish the homomer type from the heteromer type.

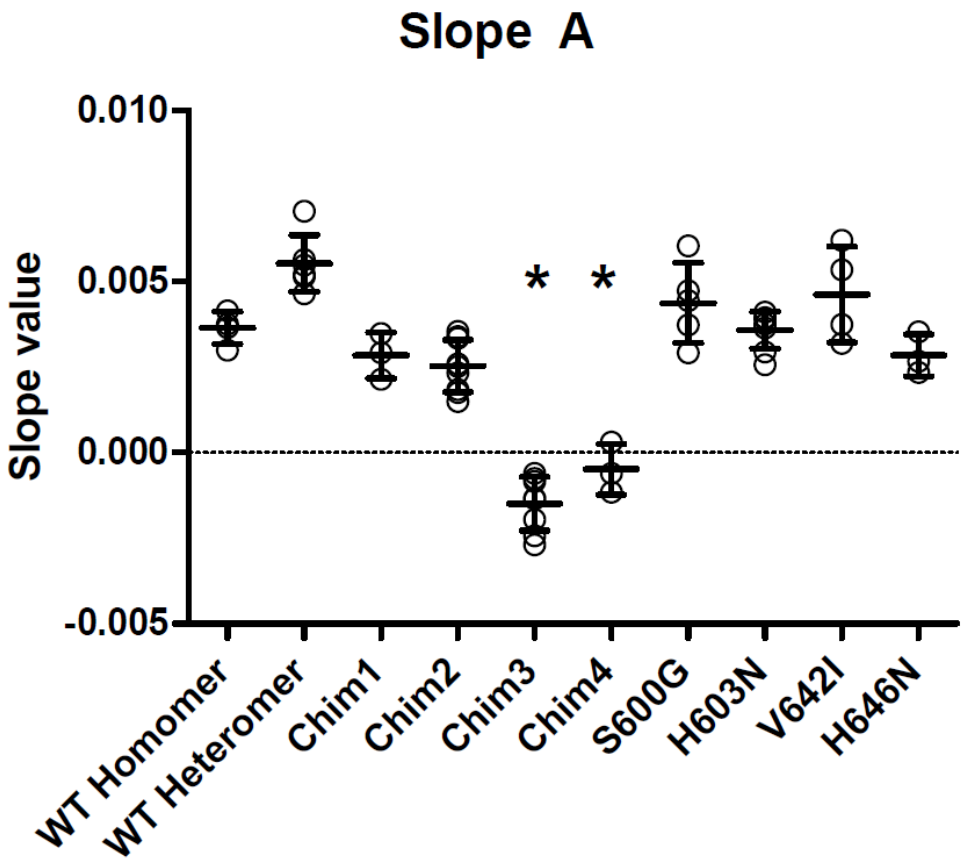


Figure 39. Comparison of the slope value A from wild type homomer, heteromer, TRPC1 mutants and chimeras. Differences in the G-V curves of chimeras 3 and 4 compared to wild type are highlighted by comparison of slopes A calculated from the G-V curves. Chimeras 3 and 4 show a significantly decreased value of slope A compared to wild type. Data are presented as mean with SD and analyzed using one-way ANOVA and Tukey's test. *$p<0.05$

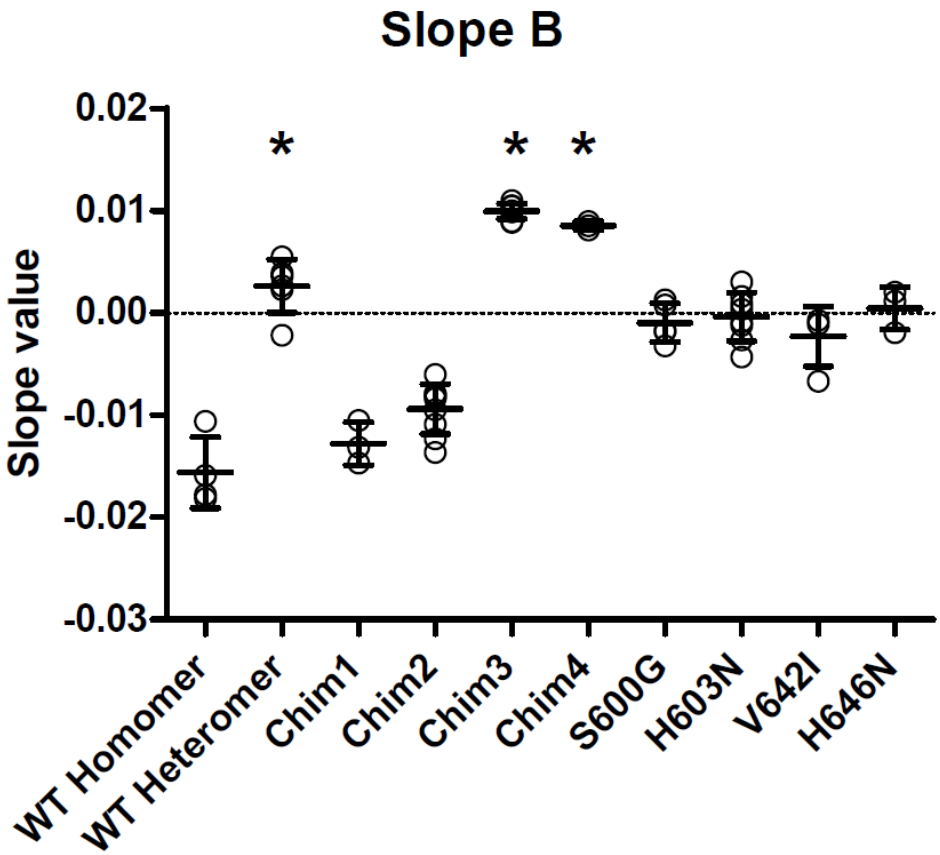


Figure 40. Comparison of the slope value B from wild type homomer, heteromer, TRPC1 mutants and chimeras. Differences in the G-V curves of chimeras 3 and 4 compared to wild type are highlighted by comparison of slopes B calculated from the G-V curves. Wild type heteromer and chimeras 3 and 4 show a significantly increased value of slope B compared to wild type homomer.

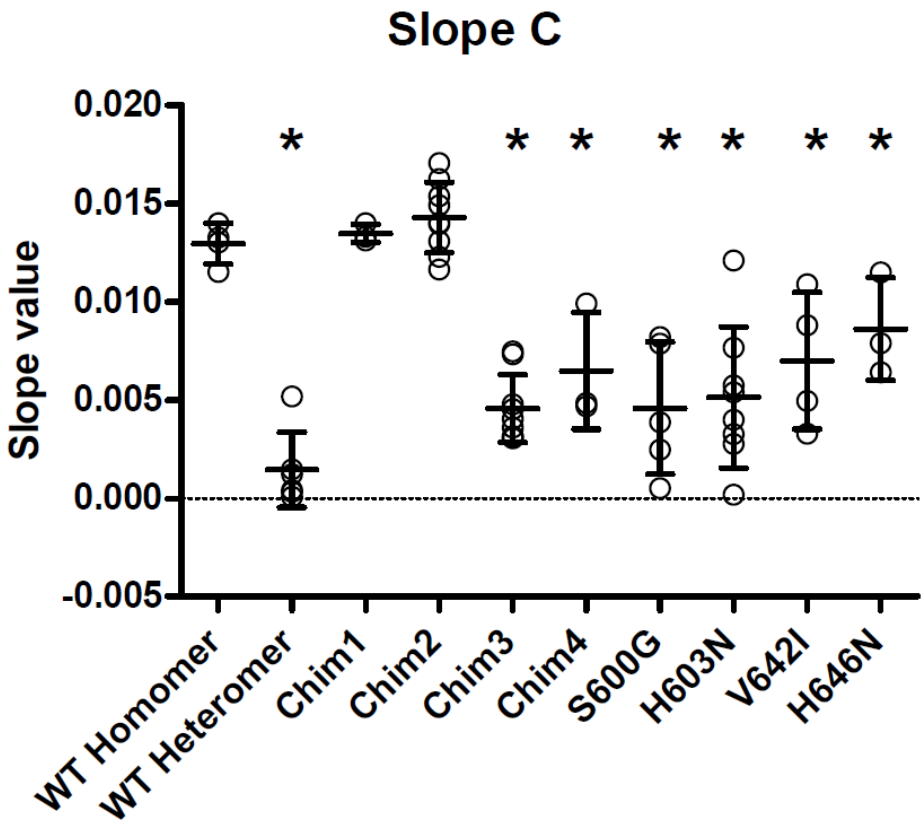


Figure 41. Comparison of the slope value C from wild type homomer, heteromer, TRPC1 mutants and chimeras. Similarity in the G-V curves of chimeras 1 and 2 compared to wild type homomer are highlighted by comparison of slopes C calculated from the G-V curves. All chimeras and mutants, except for chimeras 1 and 2, show decreased slope C value compared to wild type homomer.

TRPC1 single mutants and chimeras did not show significant current size changes compared to wild type, according to whole cell patch clamp analysis in HEK293 cells (Figure 42). In our previous studies, the ratio of current sizes at +25 mV and −60 mV, termed "rectification factor," was used to characterize the I−V shape and rectification of the TRPC1/4 heteromer channels (15). The chimeric channels 1 and 2 with the TRPC4 pores showed a significantly lower ratio (0.091 ± 0.020, n=6, 0.11 ± 0.049, n=6, 0.14 ± 0.062, n=10 for wild type TRPC4, chimera 1 and chimera 2) indicating a bigger inward current at negative membrane potentials and a block at slightly positive membrane potentials, resembling that of a TRPC4 wild type channel (Figure 43).

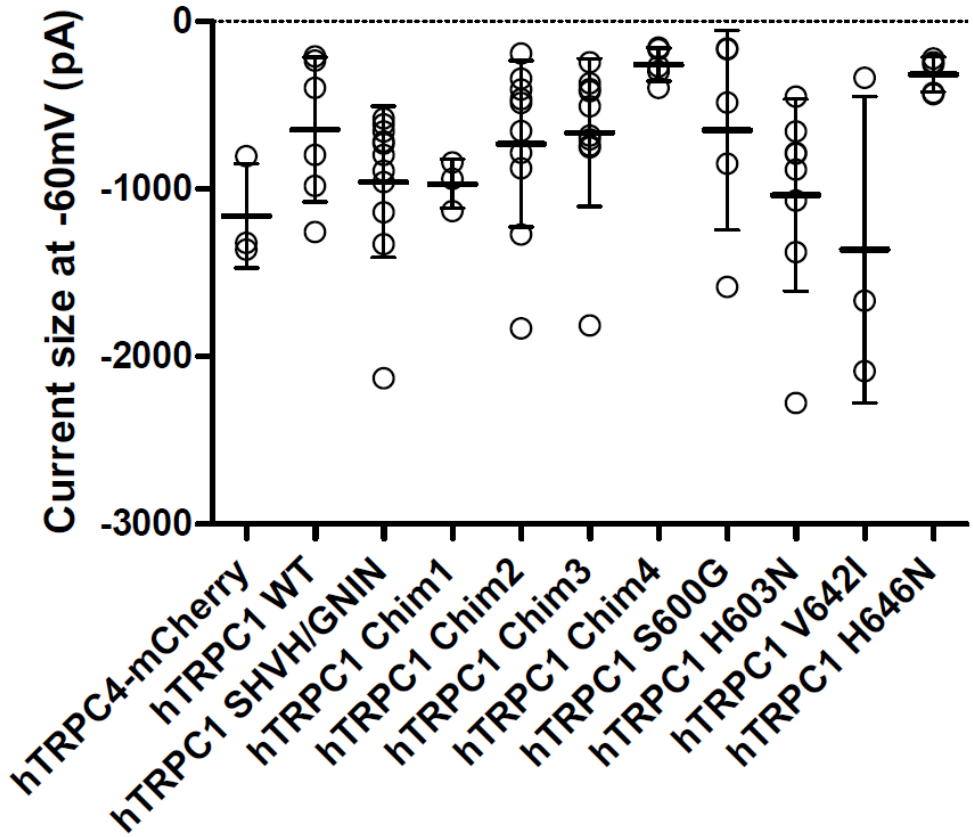


**Figure 42.** TRPC1 mutants' (co-expressed with TRPC4) current sizes at -60 mV show no significant differences among different mutants (n= 6 to 10). Data are presented as mean with SD and analyzed using one-way ANOVA and Tukey's test. *p<0.05

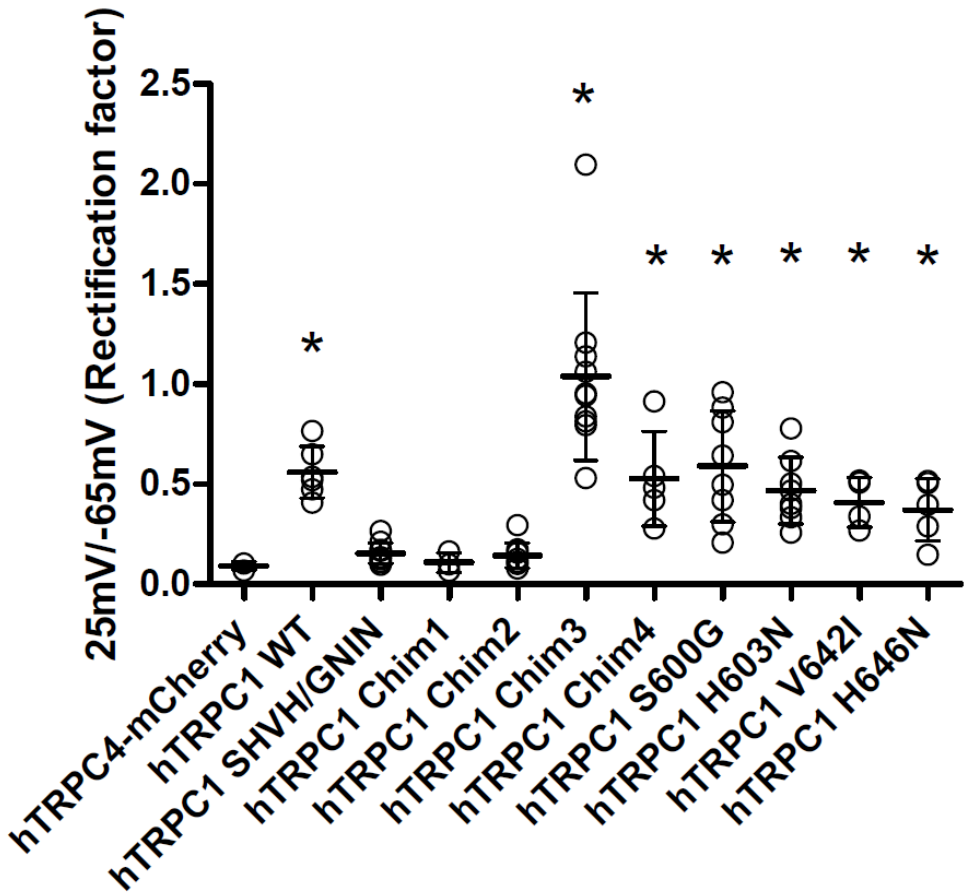


**Figure 43.** Ratios of current sizes at +25 mV and −60 mV that we termed as "rectification factor" are shown. Quadruple mutant, chimera 1 and 2 rectification factors are not significantly different from the wild type homomeric TRPC4, whereas other mutants and TRPC1/4 wild type heteromer have significantly higher ratios (n= 6 to 10). Data are presented as mean with SD and analyzed using one−way ANOVA and Tukey's test. *$p<0.05$

# 4. Discussion

## TRPC4 pore residues and calcium permeability

Here, we suggest that the pore residues of TRPC4 are important in calcium permeation, and we can reduce calcium permeability of the channel by switching these residues to that of TRPC1 identity. TRPC1 has been known to regulate calcium permeability in heteromeric channels, and decreased selectivity for calcium has been observed in previous studies (17). At first sight, the selectivity filter seems responsible for calcium permeability, particularly the S600 residue which resembles the serine residue in the bacterial voltage gated $Na^+$ channel $Na_vRh$ (47, 48). Unlike the glycine in TRPC4, the serine residue with its hydroxyl group side chain may hinder the ion permeation path, and simulations in the voltage gated $Na^+$ channel have shown that calcium permeation is energetically disfavored (48). Here in this study, we suggest that N580 and the lower gate residues are the candidate residues for affecting calcium permeability. GCaMP6s is a useful tool in that it reflects calcium permeability through TRPC4 channels, but not cytosolic increase of calcium as a whole. Measuring calcium concentration near channels is important in that it can potentiate TRPC4 channel directly, or play a role in calcium-induced calcium release (CICR) to further activate TRPC4 channels (32). As mentioned by others, V642 and H646 in TRPC1 (or I617 and N621 inTRPC4) is the most restricting region going down the pore axis (Figure 3) (34, 47). Changing these residues in TRPC4 to that of TRPC1 do not necessarily change the size of the current but do show a dramatic decrease in calcium permeability, suggesting that

selectivity for calcium is being affected (Figure 10). This is not ruling out the fact that the selectivity filter is important but also suggesting another means of controlling ion permeability in a heteromeric context. Also, changing the selectivity filter residue N580 to histidine decreased calcium permeability as shown in our results (0.82±0.15, and 0.33±0.10, wild type TRPC4 and N580 mutant, respectively) (Figure 12). To sum up our findings, mutation to a corresponding TRPC1 residue changed the channel ' s permeability to calcium according to the GCaMP6s fluorescence responses, and it emphasizes the versatility of TRPC1 containing heteromeric channels in controlling calcium permeability of the cell.

TRPC1 has been shown to control calcium release from the endoplasmic reticulum (ER) as well (16). It is worth noting that coexpression of TRPC4 or TRPC5 localizes TRPC1 at the cell membrane as a heteromer, which acts as a receptor operated channel (16). Such spatial dislocation via TRPC4 or TRPC5 may interfere with TRPC1's activity at the ER which may mediate store operated calcium entry, and affect calcium dynamics of the cell.

### TRPC4 selectivity filter mutants show altered conductance pattern

G-V curve analysis shows that mutations in the selectivity filter residues change the conductance pattern of the channel (Figure 14, 15). The GN/SH double mutant shows a G-V curve shape significantly deviating away from the observed N-shaped curve of the wild type homomeric TRPC4 channel (Figure 18). The significant difference in the slope value B suggests an increase in conductance in the depolarizing region, and this difference is again highlighted when the minimum values of the G-V curves are

compared with wild type (Figure 23, 25). Such increase in minimum conductance values in the outward rectifying region may lead to decreased excitability of the cell in a physiological context.

### S6 region of the TRPC1/4 heteromer controls outward rectification

The most striking difference we see between the TRPC1/4 heteromeric channel and other homomeric channels of TRPC4 or TRPC5 is the outward-rectifying IV curve. In our experiments, we tried to mimic the homomeric double rectifying current using single mutants of the most restricting pore residues and pore chimeras of TRPC1 and found that the single mutants are not sufficient to change the I-V curve, but the pore chimeras were able to generate curves similar to that of homomeric channels. It is critical to point out that the transition from a heteromeric I-V curve to a homomeric I-V curve starts from chimera 2, where the selectivity filter and the S6 helix without the lower gate residues are changed to that of TRPC4. When only the selectivity filter is changed in chimera 3, we see an I-V curve somewhat in between a heteromeric channel and a homomeric channel, and when even less residues are changed in chimera 4 (only residues S600 to H603), the I-V shape barely changes from the initial heteromeric I-V curve (Figure 37, 38). This seems to indicate that the S6 region is the important pore region that is controlling the shape of the outward-rectifying I-V curve in heteromeric channels. Contrary to our predictions, the selectivity filter nor the lower gate residues by themselves do not have an effect on this change in I-V curve.

The change in the I-V curve has great significance in that we see the most change in current size within the physiological range of voltage. At −60 mV, which is a resting membrane potential

for most of the excitable cells, the heteromeric TRPC1/4 channels show minimal inward current. Because these channels are mainly outward rectifying, presence of heteromeric channels in the membrane may be more responsible towards the hyperpolarizing end and render the cell less inclined to excitation via depolarization. The most striking difference that we see and perhaps the most important, is the fact that the outward current that was once blocked in the homomeric TRPC4 current is now visible in the heteromeric TRPC1/4 channels. Within this physiological range of membrane potential (0 to +40 mV), TRPC4 homomeric channels do not pass any current during what may be seen as a depolarizing event. But outward current is observed in TRPC1/4 heteromeric channels under the same conditions, suggesting that the presence and number of these channels may play a role in fine-tuning the excitability of the cell.

Such relief in the 0 to +40 mV range resembles the study in TRPC5 where a similar current block, likely due to a magnesium-induced block, is lifted with a cytosolic aspartate mutation (D633)(49). It also resembles the case with the polyamine spermine-induced block in TRPC4 governed by the residues in the C-terminal cluster (50). In addition, Obukhov and Nowycky describes that there may be additional structural differences besides D633 (N670 in TRPC1) that is responsible for the outward rectifying I-V curve in TRPC1/5 heteromeric channels, as mutating N670 to aspartate in TRPC1 by itself did not yield significant changes in the I-V curve. Considering the close homology between TRPC4 and TRPC5, we propose that other structural differences lie within the pore region of the channel.

### Limitations and future directions of the study

It is possible that the mutations themselves acting as loss-of-function mutations, and not the effect of substitution, be the cause of change in calcium permeability or the I-V curve. To rule out this possibility, further experiments where we compare the substitution mutations with alanine mutations may be needed. Because we base our assumptions on the properties of amino acids, substitution to other residues with similar moiety (asparagine to arginine or lysine in place of histidine mutation) could also be made for comparison and consolidation of the roles of these residues.

### The search for molecular and structural determinants critical for heteromer research

In summary, switching the identity of the pore residues from TRPC4 to TRPC1 can control calcium permeability, and the shape of the I-V curve depend on these pore residues (Figure 44, 45). Characterizing heteromers has been a challenge due to lack of structural studies, and here we hint at possible methods for studying heteromers along with the regions that are crucial in maintaining the characteristics of the channel, hoping to shed some light in the yet unknown area of heteromer research.

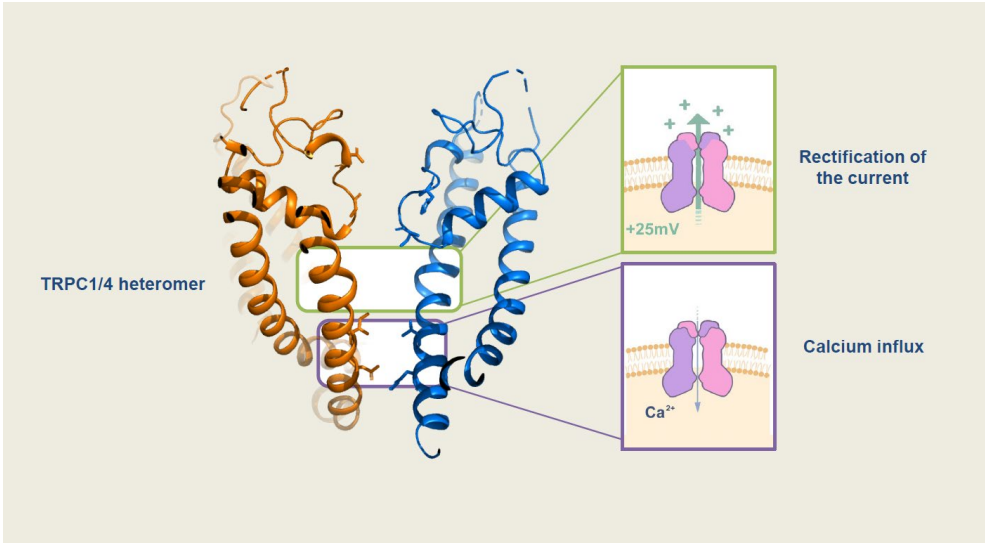


**Figure 44.** The graphical abstract showing how the pore region changes the TRPC1/4 heteromer's channel properties. The lower gate of the TRPC1/4 heteromer affects calcium permeability and the S6 helix is responsible for the shape of the channel's I-V curve.

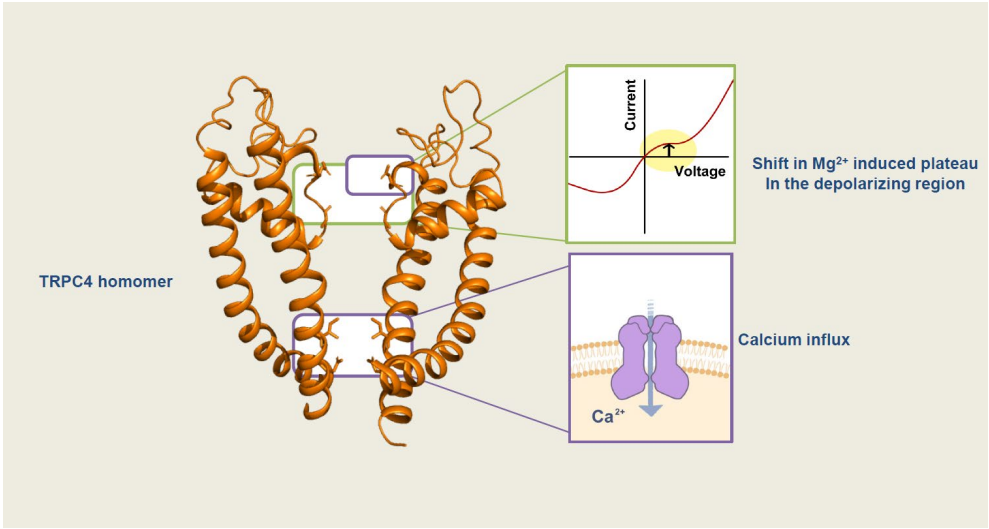


**Figure 45.** The graphical abstract showing how the pore region affects TRPC4 homomer's channel properties. The lower gate and N580 of the TRPC4 homomer affects calcium permeability and the selectivity filter is responsible for the upward shift in $Mg^{2+}$ induced plateau in the I-V curve.

# Bibliography

1. Nilius B, and Flockerzi V. *Mammalian Transient Receptor Potential (TRP) Cation Channels*. Berlin, Germany: Springer, 2014.

2. McKay RR, Szymeczek-Seay CL, Lievremont JP, Bird GS, Zitt C, Jungling E, Luckhoff A, and Putney JW, Jr. Cloning and expression of the human transient receptor potential 4 (TRP4) gene: localization and functional expression of human TRP4 and TRP3. *Biochem J* 351 Pt 3: 735-746, 2000.

3. Freichel M, Suh SH, Pfeifer A, Schweig U, Trost C, Weissgerber P, Biel M, Philipp S, Freise D, Droogmans G, Hofmann F, Flockerzi V, and Nilius B. Lack of an endothelial store-operated Ca2+ current impairs agonist-dependent vasorelaxation in TRP4-/- mice. *Nat Cell Biol* 3: 121-127, 2001.

4. Lee KP, Jun JY, Chang IY, Suh SH, So I, and Kim KW. TRPC4 is an essential component of the nonselective cation channel activated by muscarinic stimulation in mouse visceral smooth muscle cells. *Mol Cells* 20: 435-441, 2005.

5. Riccio A, Medhurst AD, Mattei C, Kelsell RE, Calver AR, Randall AD, Benham CD, and Pangalos MN. mRNA distribution analysis of human TRPC family in CNS and peripheral tissues. *Brain Res Mol Brain Res* 109: 95-104, 2002.

6. Garcia RL, and Schilling WP. Differential expression of mammalian TRP homologues across tissues and cell lines. *Biochem Biophys Res Commun* 239: 279-283, 1997.

7. Seth M, Zhang ZS, Mao L, Graham V, Burch J, Stiber J, Tsiokas L, Winn M, Abramowitz J, Rockman HA, Birnbaumer L, and Rosenberg P. TRPC1 channels are critical for hypertrophic signaling in the heart. *Circ Res* 105: 1023-1030, 2009.

8. Sours S, Du J, Chu S, Ding M, Zhou XJ, and Ma R. Expression of canonical transient receptor potential (TRPC) proteins in human glomerular mesangial cells. *Am J Physiol Renal Physiol* 290: F1507-1515,

2006.

9. Wang X, Pluznick JL, Wei P, Padanilam BJ, and Sansom SC. TRPC4 forms store-operated Ca2+ channels in mouse mesangial cells. *Am J Physiol Cell Physiol* 287: C357-364, 2004.

10. Kollewe A, Schwarz Y, Oleinikov K, Raza A, Haupt A, Wartenberg P, Wyatt A, Boehm U, Ectors F, Bildl W, Zolles G, Schulte U, Bruns D, Flockerzi V, and Fakler B. Subunit composition, molecular environment, and activation of native TRPC channels encoded by their interactomes. *Neuron* 110: 4162-4175 e4167, 2022.

11. Kim J, Ko J, Myeong J, Kwak M, Hong C, and So I. TRPC1 as a negative regulator for TRPC4 and TRPC5 channels. *Pflugers Arch* 471: 1045-1053, 2019.

12. Kim J, Ko J, Hong C, and So I. Structure-Function Relationship and Physiological Roles of Transient Receptor Potential Canonical (TRPC) 4 and 5 Channels. *Cells* 9: 2019.

13. Hofmann T, Schaefer M, Schultz G, and Gudermann T. Subunit composition of mammalian transient receptor potential channels in living cells. *Proc Natl Acad Sci U S A* 99: 7461-7466, 2002.

14. Wes PD, Chevesich J, Jeromin A, Rosenberg C, Stetten G, and Montell C. TRPC1, a human homolog of a Drosophila store-operated channel. *Proc Natl Acad Sci U S A* 92: 9652-9656, 1995.

15. Kim J, Kwak M, Jeon JP, Myeong J, Wie J, Hong C, Kim SY, Jeon JH, Kim HJ, and So I. Isoform- and receptor-specific channel property of canonical transient receptor potential (TRPC)1/4 channels. *Pflugers Arch* 466: 491-504, 2014.

16. Alfonso S, Benito O, Alicia S, Angelica Z, Patricia G, Diana K, and Vaca L. Regulation of the cellular localization and function of human transient receptor potential channel 1 by other members of the TRPC family. *Cell Calcium* 43: 375-387, 2008.

17. Storch U, Forst AL, Philipp M, Gudermann T, and Mederos y Schnitzler M. Transient receptor potential channel 1 (TRPC1) reduces calcium permeability in heteromeric channel complexes. *J Biol Chem* 287:

3530-3540, 2012.

18. Myeong J, Ko J, Hong C, Yang D, Lee KP, Jeon JH, and So I. The interaction domains of transient receptor potential canonical (TRPC)1/4 and TRPC1/5 heteromultimeric channels. *Biochem Biophys Res Commun* 474: 476-481, 2016.

19. Wang HS, Pan Z, Shi W, Brown BS, Wymore RS, Cohen IS, Dixon JE, and McKinnon D. KCNQ2 and KCNQ3 potassium channel subunits: molecular correlates of the M-channel. *Science* 282: 1890-1893, 1998.

20. Hanaoka K, Qian F, Boletta A, Bhunia AK, Piontek K, Tsiokas L, Sukhatme VP, Guggino WB, and Germino GG. Co-assembly of polycystin-1 and -2 produces unique cation-permeable currents. *Nature* 408: 990-994, 2000.

21. Bai CX, Giamarchi A, Rodat-Despoix L, Padilla F, Downs T, Tsiokas L, and Delmas P. Formation of a new receptor-operated channel by heteromeric assembly of TRPP2 and TRPC1 subunits. *EMBO Rep* 9: 472-479, 2008.

22. Broker-Lai J, Kollewe A, Schindeldecker B, Pohle J, Nguyen Chi V, Mathar I, Guzman R, Schwarz Y, Lai A, Weissgerber P, Schwegler H, Dietrich A, Both M, Sprengel R, Draguhn A, Kohr G, Fakler B, Flockerzi V, Bruns D, and Freichel M. Heteromeric channels formed by TRPC1, TRPC4 and TRPC5 define hippocampal synaptic transmission and working memory. *EMBO J* 36: 2770-2789, 2017.

23. Malarkey EB, Ni Y, and Parpura V. Ca2+ entry through TRPC1 channels contributes to intracellular Ca2+ dynamics and consequent glutamate release from rat astrocytes. *Glia* 56: 821-835, 2008.

24. Phelan KD, Mock MM, Kretz O, Shwe UT, Kozhemyakin M, Greenfield LJ, Dietrich A, Birnbaumer L, Freichel M, Flockerzi V, and Zheng F. Heteromeric canonical transient receptor potential 1 and 4 channels play a critical role in epileptiform burst firing and seizure-induced neurodegeneration. *Mol Pharmacol* 81: 384-392, 2012.

25. Phelan KD, Shwe UT, Abramowitz J, Wu H, Rhee SW, Howell MD, Gottschall PE, Freichel M, Flockerzi V, Birnbaumer L, and Zheng F.

Canonical transient receptor channel 5 (TRPC5) and TRPC1/4 contribute to seizure and excitotoxicity by distinct cellular mechanisms. *Mol Pharmacol* 83: 429-438, 2013.

26. Sung HH, Choo SH, Ko M, Kang SJ, Chae MR, Kam SC, Han DH, So I, and Lee SW. Increased expression of TRPC4 channels associated with erectile dysfunction in diabetes. *Andrology* 2: 550-558, 2014.

27. Sabourin J, Bartoli F, Antigny F, Gomez AM, and Benitah JP. Transient Receptor Potential Canonical (TRPC)/Orai1-dependent Store-operated Ca2+ Channels: NEW TARGETS OF ALDOSTERONE IN CARDIOMYOCYTES. *J Biol Chem* 291: 13394-13409, 2016.

28. Sabourin J, Boet A, Rucker-Martin C, Lambert M, Gomez AM, Benitah JP, Perros F, Humbert M, and Antigny F. Ca(2+) handling remodeling and STIM1L/Orai1/TRPC1/TRPC4 upregulation in monocrotaline-induced right ventricular hypertrophy. *J Mol Cell Cardiol* 118: 208-224, 2018.

29. Malczyk M, Veith C, Fuchs B, Hofmann K, Storch U, Schermuly RT, Witzenrath M, Ahlbrecht K, Fecher-Trost C, Flockerzi V, Ghofrani HA, Grimminger F, Seeger W, Gudermann T, Dietrich A, and Weissmann N. Classical transient receptor potential channel 1 in hypoxia-induced pulmonary hypertension. *Am J Respir Crit Care Med* 188: 1451-1459, 2013.

30. Muraki K, Ohnishi K, Takezawa A, Suzuki H, Hatano N, Muraki Y, Hamzah N, Foster R, Waldmann H, Nussbaumer P, Christmann M, Bon RS, and Beech DJ. Na(+) entry through heteromeric TRPC4/C1 channels mediates (-)Englerin A-induced cytotoxicity in synovial sarcoma cells. *Sci Rep* 7: 16988, 2017.

31. Ludlow MJ, Gaunt HJ, Rubaiy HN, Musialowski KE, Blythe NM, Vasudev NS, Muraki K, and Beech DJ. (-)-Englerin A-evoked Cytotoxicity Is Mediated by Na+ Influx and Counteracted by Na+/K+-ATPase. *J Biol Chem* 292: 723-731, 2017.

32. Ko J, Myeong J, Yang D, and So I. Calcium permeability of transient receptor potential canonical (TRPC) 4 channels measured by

TRPC4-GCaMP6s. *Korean J Physiol Pharmacol* 21: 133-140, 2017.

33. Jeon JP, Roh SE, Wie J, Kim J, Kim H, Lee KP, Yang D, Jeon JH, Cho NH, Kim IG, Kang DE, Kim HJ, and So I. Activation of TRPC4beta by Galphai subunit increases Ca2+ selectivity and controls neurite morphogenesis in cultured hippocampal neuron. *Cell Calcium* 54: 307-319, 2013.

34. Duan J, Li J, Zeng B, Chen GL, Peng X, Zhang Y, Wang J, Clapham DE, Li Z, and Zhang J. Structure of the mouse TRPC4 ion channel. *Nat Commun* 9: 3102, 2018.

35. Lee JE. The roles of pore-lining residues in the physiological properties of TRPC4: response to G protein and voltage-dependency. In: *Biomedical Sciences*Seoul National University, 2022.

36. Xian W. Structural and functional characterisation of TRP channels. Universität des Saarlandes, 2018.

37. Nadezhdin KD, Neuberger A, Nikolaev YA, Murphy LA, Gracheva EO, Bagriantsev SN, and Sobolevsky AI. Extracellular cap domain is an essential component of the TRPV1 gating mechanism. *Nat Commun* 12: 2154, 2021.

38. Yang F, Xu L, Lee BH, Xiao X, Yarov-Yarovoy V, and Zheng J. An Unorthodox Mechanism Underlying Voltage Sensitivity of TRPV1 Ion Channel. *Adv Sci (Weinh)* 7: 2000575, 2020.

39. Lolicato M, Arrigoni C, Mori T, Sekioka Y, Bryant C, Clark KA, and Minor DL, Jr. K(2P)2.1 (TREK-1)-activator complexes reveal a cryptic selectivity filter binding site. *Nature* 547: 364-368, 2017.

40. Ben Soussia I, El Mouridi S, Kang D, Leclercq-Blondel A, Khoubza L, Tardy P, Zariohi N, Gendrel M, Lesage F, Kim EJ, Bichet D, Andrini O, and Boulin T. Mutation of a single residue promotes gating of vertebrate and invertebrate two-pore domain potassium channels. *Nat Commun* 10: 787, 2019.

41. Schewe M, Nematian-Ardestani E, Sun H, Musinszki M, Cordeiro S, Bucci G, de Groot BL, Tucker SJ, Rapedius M, and Baukrowitz T. A Non-canonical Voltage-Sensing Mechanism Controls Gating in K2P K(+)

Channels. *Cell* 164: 937-949, 2016.

42. Rietmeijer RA, Sorum B, Li B, and Brohawn SG. Physical basis for distinct basal and mechanically gated activity of the human K(+) channel TRAAK. *Neuron* 109: 2902-2913 e2904, 2021.

43. Yu X, Xie Y, Zhang X, Ma C, Liu L, Zhen W, Xu L, Zhang J, Liang Y, Zhao L, Gao X, Yu P, Luo J, Jiang LH, Nie Y, Yang F, Guo J, and Yang W. Structural and functional basis of the selectivity filter as a gate in human TRPM2 channel. *Cell Rep* 37: 110025, 2021.

44. Strubing C, Krapivinsky G, Krapivinsky L, and Clapham DE. TRPC1 and TRPC5 form a novel cation channel in mammalian brain. *Neuron* 29: 645-655, 2001.

45. Erickson MG, Alseikhan BA, Peterson BZ, and Yue DT. Preassociation of calmodulin with voltage-gated Ca(2+) channels revealed by FRET in single living cells. *Neuron* 31: 973-985, 2001.

46. Akbulut Y, Gaunt HJ, Muraki K, Ludlow MJ, Amer MS, Bruns A, Vasudev NS, Radtke L, Willot M, Hahn S, Seitz T, Ziegler S, Christmann M, Beech DJ, and Waldmann H. (-)-Englerin A is a potent and selective activator of TRPC4 and TRPC5 calcium channels. *Angew Chem Int Ed Engl* 54: 3787-3791, 2015.

47. Bacsa B, Tiapko O, Stockner T, and Groschner K. Mechanisms and significance of Ca(2+) entry through TRPC channels. *Curr Opin Physiol* 17: 25-33, 2020.

48. Zhang X, Xia M, Li Y, Liu H, Jiang X, Ren W, Wu J, DeCaen P, Yu F, Huang S, He J, Clapham DE, Yan N, and Gong H. Analysis of the selectivity filter of the voltage-gated sodium channel Na(v)Rh. *Cell Res* 23: 409-422, 2013.

49. Obukhov AG, and Nowycky MC. A cytosolic residue mediates Mg2+ block and regulates inward current amplitude of a transient receptor potential channel. *J Neurosci* 25: 1234-1239, 2005.

50. Kim J, Moon SH, Shin YC, Jeon JH, Park KJ, Lee KP, and So I. Intracellular spermine blocks TRPC4 channel via electrostatic interaction with C-terminal negative amino acids. *Pflugers Arch* 468: 551-561, 2016.

# Abstract

TRPC1과 TRPC4는 같은 TRPC채널과에 속해있는 단백질로, 둘은 함께 결합하여 헤테로사량체를 만들 수 있는 것으로 알려져 있다. TRPC4는 자체적으로 호모사량체 비선택적 양이온 채널을 만들 수 있으나, TRPC1가 포함되면 이온통로의 주요 성질들이 변하게 된다. 본 연구에서는 채널의 통로 부분(선택성 필터, pore helix, S6 helix)의 아미노산 잔기가 TRPC1/4 이형복합체 이온통로의 성질을 결정한다고 예상하고, 키메라와 돌연변이를 통해 이온통로의 칼슘 투과도와 I-V 관계의 변화를 관찰하였다. 비슷한 아미노산 서열을 갖고 있는 TRPC4와 TRPC5의 구조가 최근에 밝혀져 pore를 구성하는 아미노산들이 알려졌다. 이를 근거로 TRPC1의 pore를 구성할 것으로 예상되는 아미노산들을 찾아내어 이를 집중적으로 연구하였다. 선택성 필터와 S6 lower gate의 기능도 비교해보기 위해 여러가지 키메라들을 만들어 실험을 진행하였다. TRPC4와 이형복합체의 키메라와 변이체의 전류를 whole-cell 패치클램프를 사용해 측정하고, GCaMP6s 형광을 사용하여 칼슘 투과도를 측정하였을 때, lower gate의 변이체들 (I617V와 N621H)은 감소한 칼슘 투과도를 보이는 것으로 확인되었다. 반면에 선택성 필터 변이체들(G577S와 N580H)은 칼슘투과도를 보였고 G577S 변이체는 정상과 별차이가 없이 칼슘이 잘 통과하였고 N580H는 정상보다는 칼슘투과도가 감소하였다. Outward-rectifying I-V 그래프를 만드는 통로 부위를 살펴보기 위해 TRPC1의 여러 통로 부위를 TRPC4로 치환한 키메라 이온통로들을 제작하였고, whole-cell 패치클램프를 통해 S6 helix가 I-V

그래프의 모양을 바꾸는 것으로 확인할 수 있었다. 이를 통해 TRPC1/4 이형복합체의 pore region이 이온통로의 특성에 관여하는 것을 알 수 있었고, 특히 이온선택성에 선택성 필터가 주된 역할을 한다고 알려져 왔지만 S6 lower gate 영역도 칼슘투과도에 관여하였다. 최근에 gate와 관련해서 S6 lower gate이외에 선택성 필터도 관여한다고 인정되는 것과 유사하게 이온투과도도 선택성 필터만 관여하는 것이 아니라 S6를 포함하여 이온통과부위 내측벽 잔기들의 복잡한 작용으로 일어난다고 볼 수 있다. 이는 앞으로의 TRPC1/4뿐 아닌 다른 이형복합체 연구에도 도움이 될 것으로 예상된다.

키워드: TRPC4, TRPC1, TRP 이형복합체, 이온통로